PAUL SCHERRER INSTITUT

# SwissFEL X-ray Free Electron Laser

## Workshops on Hard X-Ray Instrumentation at the SwissFEL
## 12.9.2011 and 21.11.2011
## University of Bern

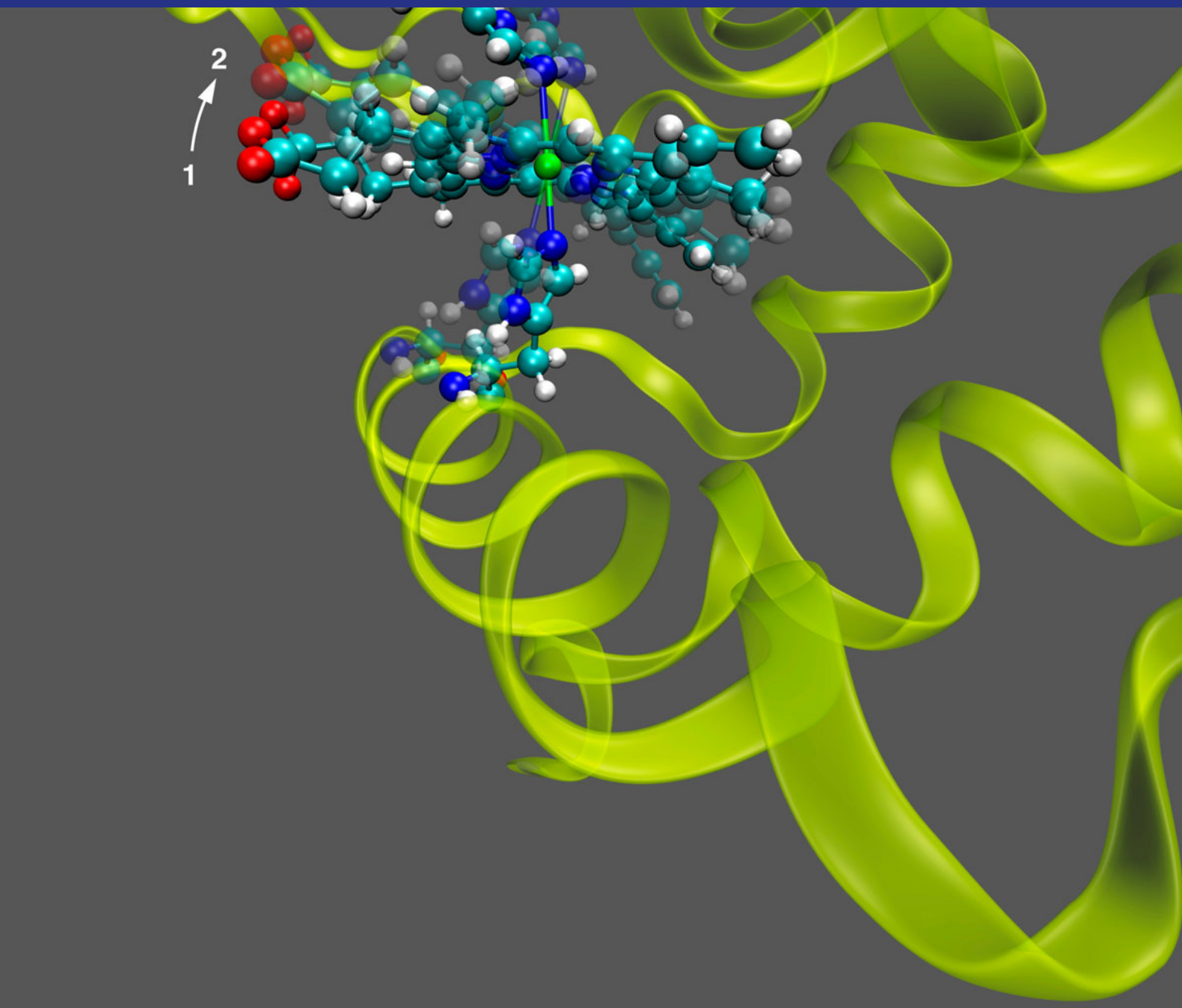


# Poster Book for Workshop Participants

Cover figure:
Courtesy of M. Meuwly, University of Basel



# Poster Presentations

## Workshop 12.09.2011

**Poster # 1**
*W. Gawelda*, A. Galler, C. Bressler
Simultaneous Ultrafast X-ray Spectroscopy and Scattering at Current and Future Lightsources

**Poster # 2**
*C. P. Hauri*, F. Ardana, C. Ruchert, A. Trisorio, C. Vicario
Pump-probe laser systems at SwissFEL for ARAMIS hard X-ray beamlines

**Poster # 3**
*A. Ichsanow*, H. Sigg, C. P. Hauri, J. Sá, J. A. van Bokhoven, B. Patterson
Initiation of catalytic reactions by THz pulses and characterization of short-lived intermediate states by X-rays

**Poster # 4**
*P. Juranić*, R. Ischebeck, V. Schlott
The Basic Concepts of Photon Beam Diagnostics in the SwissFEL Tunnel Front End

**Poster # 5**
*C. J. Milne*
Electronic and Structural Dynamics in Solution: Pump-Probe XAS, XES, RIXS

**Poster # 6**
*A. Mozzanica*, A. Bergamaschi, R. Dinapoli, D. Greiffenberg, B. Henrich, I. Johnson, D. Maliakal, C. Ruder, B. Schmitt, X. Shi
Adaptive gain charge integrating detectors for SwissFEL

**Poster # 7**
P. Oberta, U. Flechsig
The preliminary optics design of the Aramis undulator beamline of the SwissFEL

**Poster # 8**
*B. Patterson*, R. Abela, B. Pedrini
Stimulated Resonant Inelastic X-Ray Scattering

**Poster # 9**
*B. Patterson*, R. Abela, B. Pedrini
Mössbauer Spectroscopic Methods at the SwissFEL

**Poster # 10**
*J. Sá*, M. Nachtegaal, J. Szlachetko, O. V. Safonova, J. A. van Bokhoven
Photocatalytic conversion of $CO_2$ to hydrocarbons over metal doped $TiO_2$ Artificial Photosynthesis

**Poster # 11**
*J. Szlachetko*, M. Nachtegaal, J. Sá, J.-C. Dousse, J. Hoszowska, M. Janousch, O. V. Safonova, A. Bergamaschi, B. Schmitt, E. De Boni, J. A. van Bokhoven
Single-shot X-ray emission spectroscopy

**Poster # 12**
*R. Thierry*, B. Gipson, H. Stahlberg
Constrained optimization methods for the retrieval of structural information in electron crystallography with limited tilt angles

## Workshop 21.11.2011

**Poster # 13**
*F. Carbone*
Multidimensional high energy experiments with X-rays and electron pulses

**Poster # 14**
*T. Penfold*, I. Tavernelli, R. Abela, M. Chergui
Ultrafast anisotropic X-ray scattering in the condensed phase

**Poster # 15**
*A. Caviezel*, P. Beaud, S. Mariager, S. Grübel, J. A. Johnson, G. Ingold
Ultrafast Structural Dynamics in Strongly Correlated Electron Systems: Timing Specifications

**Poster # 16**
*A. Caviglia*, M. Först, R. Scherwitzl, J.-M. Triscone, A. Cavalleri
Vibrational control of quantum materials: ultrafast X-ray diffraction studies

**Poster # 17**
*J. A. Johnson*, S. Grübel, S. O. Mariager, A. Caviezel, P. Beaud, G. Ingold
Coherent Control of Microscopic Order: high field THz and X-ray experiments at the SwissFEL

**Poster # 18**
*T. Huber*, S. Johnson
Time-resolved Diffuse X-ray Scattering

**Poster # 19**
*F. Stellato*, K. Nass, S. Bajt, C. Caleman, D. DePonte, A. V. Martin, T. A. White, A. Barty, H. N. Chapman
Serial Femtosecond Crystallography at SwissFEL X-Ray Free Electron Laser

**Poster # 20**
*S. O. Mariager*, P. Beaud, A. Caviezel, S. Grübel, J. A. Johnson, G. Ingold, U. Staub, V. Scagnoli, S. L. Johnson, L. LeGuyader, F. Nolting, C. Quitman
Probing magnetic phase transitions

**Poster # 21**
*C. Cozzo*, M. Cabanes-Sempere, M. A. Pouchon, S. Vaucher, R. Nicula
Influence of gelation kinetics by microwaves

**Poster # 22**
*A Froideval*, J. Chen, C. Degueldre, M. Krack, G. Kuri, M. Martin, S. Portier, M. A. Pouchon, B. D. Patterson
Dynamics of irradiation-induced defects in nuclear materials: a proposed energetic-ion pump - X-ray FEL probe experimental approach

**Poster # 23**
*P. Karvinen*, S. Rutishauser, S. Gorelick, A. Mozzanica, D. Greiffenberg, J. Krzywinski, D. M. Fritz, H. T. Lemke, M. Cammarata, C. David
Diffractive optics for focusing and characterization of X-ray free electron laser radiation

**Poster # 24**
*A. Rudenko*, S. Epp, D. Rolles, R. Hartmann, L. Foucar, B. Rudek, B. Erk, F. Krasniqi, L. Strüder, I. Schlichting, J. Ullrich
CAMP: Flexible User End Station for Multidimensional Imaging Experiments at XFELs

**Poster # 25**
*V. Panneels*, C.-J. Tsai, X.-D. Li, G. Capitani, M. Steinmetz, G. Schertler
Femtosecond analysis of protein nanocrystals and supramolecular complexes

**Poster # 26**
*D. Bleiner*, F. Staub, J. E. Ballmer, Th. Feurer
Table-top Soft X-ray Laser in the X-ray Free-Electron Laser Era

**Poster # 27**
S. Prabakharan, *V. Roth*
Inferring Networks from Distances: The “Landscape” of Glycosidase Protein Structures

**Poster # 28**
*S. J. Leake*
Bragg CDI at an XFEL

**Poster # 29**
*J. Steinbrener*, L. Lomb, D. Rolles, F. Krasniqi, M. Hartmann, L. Strüder, J. Ullrich, I. Schlichting, T. R. M. Barends, S. Kassemeyer, A. Jafarpour, R. Shoeman, S. Bari, S. Epp, L. Foucar, A. Rudenko
Serial Femtosecond Crystallography on tiny 3D crystals

**Poster # 30**
*G. Pigino*, A. Maheshwari, B. Malkova, T. Ishikawa
Electron Cryo-microscopy and tomography of eukaryotic cilia/flagella

**Poster # 31**
S. V. Churakov, *R. Dähn*, A. Froideval, B. Pedrini
Dynamics of ion diffusion in clays: a proposed probe - probe XPCS experiment

**Poster # 32**
D. Müller, *C. Bühler*
Selected Applications on Data-Intense Research

**Poster # 33**
*S. Johnson*
Possibilities for nonlinear x-ray scattering with SwissFEL

**Poster # 34**
C.-J. Tsai, *B. Pedrini*, C. M. Kewish, B. Patterson, R. Abela, G. Schertler, X.-D. Li
2D Membrane Protein Crystal Diffraction

**Poster # 35**
*J. J. Szymczak*, F. Hofmann, M. Meuwly
Energetics and Solvation Dynamics of the excited $Ru(bpy)_3$ complex in water

## Poster # 1

W. Gawelda, A. Galler, C. Bressler

**Simultaneous Ultrafast X-ray Spectroscopy and Scattering at Current and Future Lightsources**

Poster follows

**Poster # 2**

PAUL SCHERRER INSTITUT

# Pump-probe laser systems at SwissFEL for ARAMIS hard X-ray beamlines

SwissFEL

*C.P. Hauri[1,2], F. Ardana[1,2], C. Ruchert[1], A.Trisorio[1], C. Vicario[1]*
*[1]Paul Scherrer Institute, 5232 Villigen, Switzerland*
*[2]Ecole Polytechnique Federale de Lausanne, Lausanne, Switzerland*

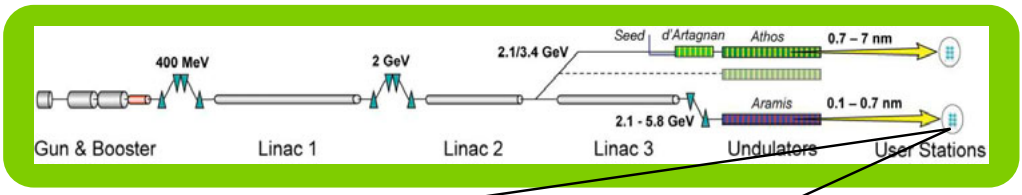


## Requirements

- low timing jitter FEL ⇔ pump/probe laser
- characterize temporal jitter shot-to-shot
- large wavelength range to be covered (THz...VIS....DUV...soft x-rays)
- multi-cycle and single-cycle pulses, pulse trains
- carrier-envelope phase stabilized pulses
- long beam path from laserhutch to EHs (up to 40 m)
- high stability and flexibility at user station
- endurance

## laser system

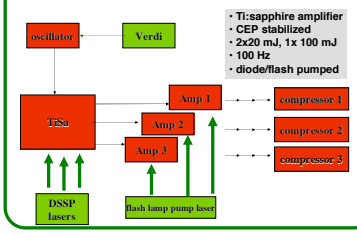


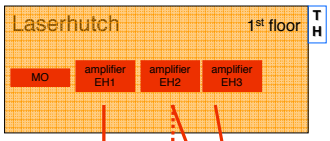


## User information/control

online diagnostics and control at experiment
- single shot pulse energy
- beam pointing/beam position
- timing jitter
- pump probe delay
- CEP phase
- temporal and spatial profile

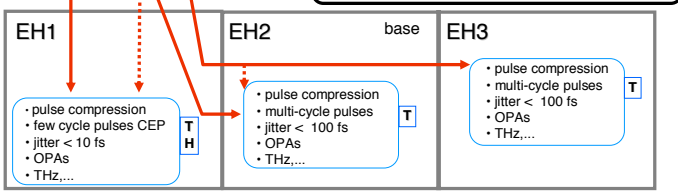


## Laser characteristics

| | | | |
|---|---|---|---|
| energy stability | | < 1-2% | required for OPAs |
| timing jitter | | 100 fs | for EH2 and EH3 |
| | | <10 fs | for EH1 |
| wavelength ranges | 750-850 nm | 20 mJ | fundamental laser wavelength Ti:sapphire |
| | 200-1000 nm | 0...1mJ | **SC**, MC |
| | **1-20 um** | 0...500 µJ | **SC**, MC |
| | 1-15 THz | 0...20 uJ | **HC, SC**, MC |
| repetition rate | | 0...100 Hz | |
| field-sensitive experiments | | yes | **CEP stabilization** in EH1 |
| power level | | 20 mJ | 1 line (freq. conversion) |
| | | 20 mJ | 1 line (SC pulse generation) |
| | | >>20 mJ | 1 line (THz) |

HC: half cycle pulses, SC: single cycle pulses,MC: multi cycle pulses

## THz source at SwissFEL

- independent THz source for SwissFEL foreseen
- THz synchronized to hard x-ray for experiments and diagnostics
- either laser-based or accelerator-based approach
- both schemes currently under investigation

### linac-based THz generation

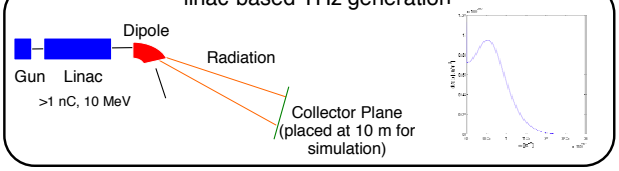


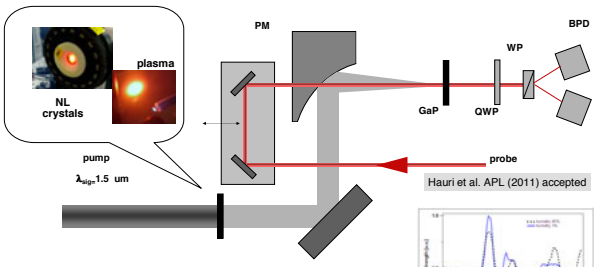


Hauri et al. APL (2011) accepted

- several MV/cm, > 1 Tesla
- single cycle/half cycle pulses of < 1 ps
- THz pump pulse up to 1 ns prio to x-ray probe pulse

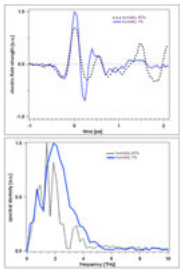

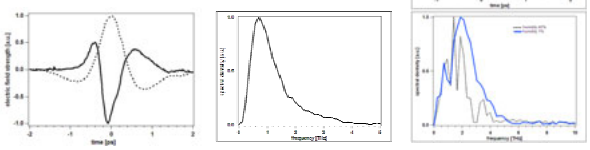

### Hard x-ray pulse characterization

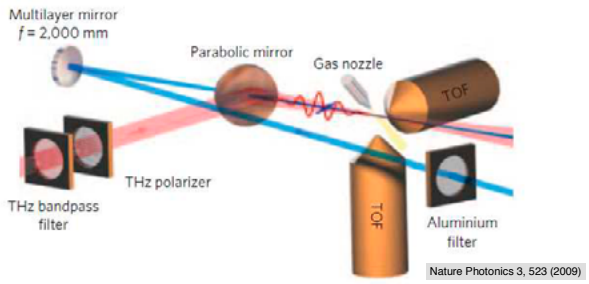


Nature Photonics 3, 523 (2009)

- single-shot FEL pulse duration
- time structure of FEL pulse
- single shot jitter monitor FEL pulse vs pump/probe laser
- arrival time monitor (sidebands)
- proven for soft x-ray FELs

**Poster # 3**

# Initiation of catalytic reactions by THz pulses and characterization of short-lived intermediate states by X-rays

SwissFEL

*Anastasija Ichsanow, Hans Sigg, Christoph Hauri, Jacinto Sá, Jeroen van Bokhoven, Bruce Patterson*
*Paul Scherrer Institute, 5232 Villigen PSI, Switzerland*

## Introduction

- 80% of all important chemical reactions take place on interfaces
- Catalytic processes vital to the chemical industry

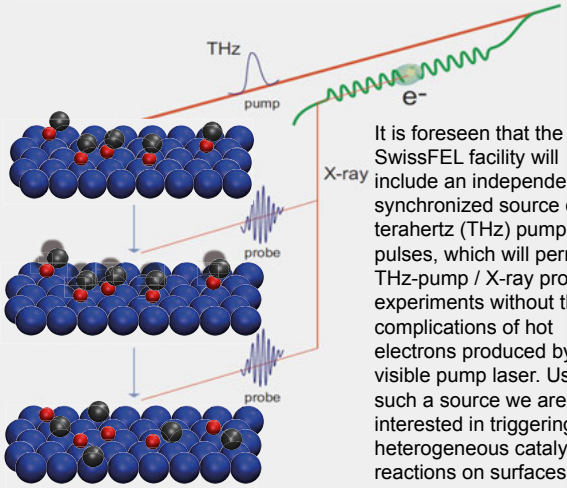


It is foreseen that the SwissFEL facility will include an independent, synchronized source of terahertz (THz) pump pulses, which will permit THz-pump / X-ray probe experiments without the complications of hot electrons produced by a visible pump laser. Using such a source we are interested in triggering heterogeneous catalytic reactions on surfaces [1,2].

## THz-pump

Catalytic reactions may be collectively initiated by the interaction of the THz electric-field with polar molecules adsorbed on a surface.

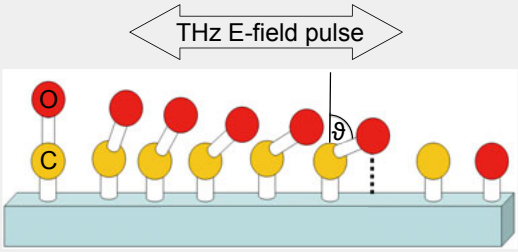


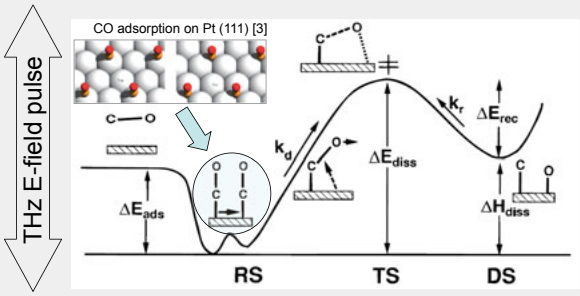


(Top) Schematic representation of THz induced dissociation of CO on a Pt surface.
(Bottom) Schematic energy-level diagram for the dissociation process. The notation corresponds to reactant (RS), dissociated (DS) and transition (TS) states [4].

## THz pulse generated by non-linear optics in a plasma

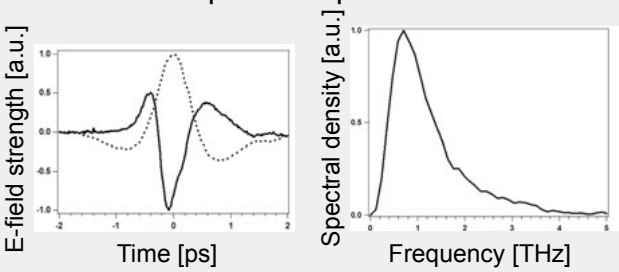


(Left) Tunable polarizability of a single cycle THz pulse.
(Right) Pulse frequency distribution around 1 THz.

@ PSI: > 1 MV/cm, ~ 10 µJ, ~ 1 mm$^2$ [5]

## X-ray-probe (NEXAFS)

Near Edge X-ray Absorption Fine Structure spectroscopy

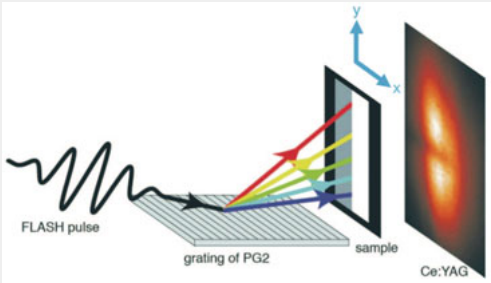


Femtosecond X-ray pulses disperse on the monochromator grating and pass through the sample. The sample is segmented for simultaneous absorption and reference measurements. The transmitted X-rays are converted into visible light on a Ce:YAG crystal and imaged with an ICCD [6].

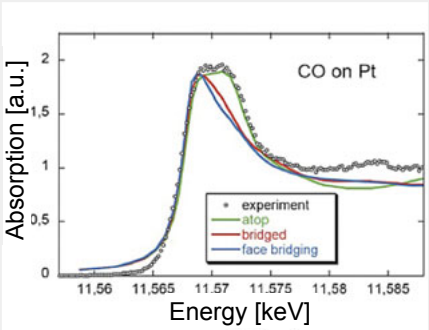


Using a single-shot probe pulse, a time-resolved NEXAFS spectrum can be collected. The spectrum reflects the instantaneous atomic and electronic structure of the system under study. The figure shows a static measurement [7].

## References

[1] Ogasawara *et al.*, JACoW / eConf C 0508213 (2005)
[2] B. Patterson *et al.*, Chimia **65**, 323 (2011)
[3] Schimka *et al.*, Nature Mater. **9**, 741 (2010)
[4] M. A. van Daelen *et al.*, J. Phys. Chem. **100,** 2279 (1996)
[5] C. Ruchert *et al.*, Chimia **65**, 320 (2011)
[6] D. P. Bernstein *et al.*, App. Phys. Let. **95**, 134102 (2009)
[7] O. Safonova *et al.*, J. Phys. Chem. B **110**, 16162 (2006)

**Poster # 4**

PAUL SCHERRER INSTITUT

SwissFEL

# The Basic Concepts for Photon Beam Diagnostics in the SwissFEL Tunnel Front End

*Pavle Juranić*, Rasmus Ischebeck, Volker Schlott*
*Paul Scherrer Institute, 5232 Villigen PSI, Switzerland*

**Abstract:**

Non-destructive, pulse-to-pulse measurements of pulse energy, photon wavelength, pulse arrival time, and pulse length are necessary for many experiments at the future SwissFEL, and are also beneficial as feedback to the operators to monitor and improve the performance of the machine that generates the FEL light. This poster will present the basic concepts and layout of the photon beam diagnostics that will be placed in the front end of the SwissFEL tunnel, providing a general overview of the devices that will be available, and their expected accuracy. Most of the devices that will be presented will use gases' interaction with light to provide the information to FEL users and operators, and will also include gas and solid attenuators to allow the users a wide range of beam intensities.

## Beam Intensity Monitor

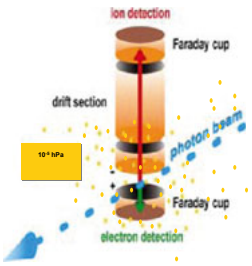


- Already used at FLASH as the FLASH gas monitor detector (GMD) (shown above).
- Will measure the intensity of the FEL beam per pulse.
- Will be gas-based, i.e. non-destructive to the FEL beam.
- FLASH is developing the new GMD for the European XFEL.

## Beam Position Monitor

MCP/Chain Anode

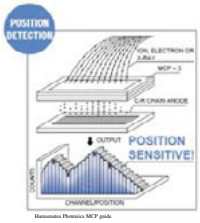


Hamamatsu Photonics MCP guide

Split Diode

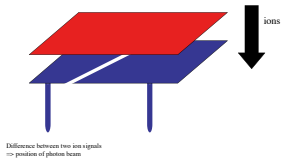


Difference between two ion signals => position of photon beam

MCP/Phosphor Screen

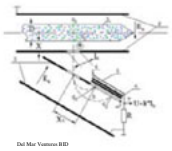

Del Mar Ventures BID

Electron-Sensitive Diodes

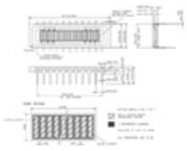

Opto Diode AXUV20EL

Many options being tested to get the best possible resolution for the expected 100 $\mu$m fwhm diameter of the SwissFEL beam in the tunnel.

## Photon Pulse Arrival Time and Length Measurement

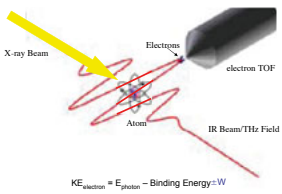


$KE_{electron} = E_{photon} - \text{Binding Energy} \pm W$

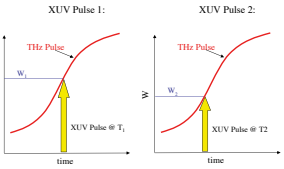


$W_2 - W_1 \Rightarrow T_2 - T_1$

The device will use THz streaking of the ionized electrons to determine the jitter between pulses, and to measure the pulse length of each individual pulse (see R. Ischebeck's poster for more information).

## Photon Wavelength Measurement

### Zone Plates

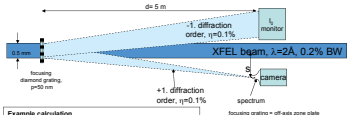


**Example calculation**

| | |
|---|---|
| diffraction angle: | $\alpha = \lambda/p = 4$ mrad |
| separation: | $s = d \times \alpha = 20$ mm |
| width of spectrum @ 0.2% BW: | $w = 0.2\% \times s = 40$ µm |
| diffraction limit of spectral resolution (equal to number of lines): | $\lambda/\delta\lambda = 10'000$ |
| required camera pixel size to reach diffraction limited resolution: | $w = s/(\lambda/\delta\lambda) = 2$ µm |

focusing grating + off-axis zone plate

Christian David, private communication

### Electron TOFs

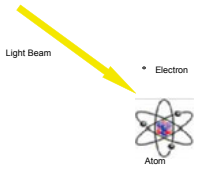


$KE_{electron} = E_{photon} - \text{Binding Energy}$

| Device | E-TOF | Zone Plate |
|---|---|---|
| Pulse Resolved? | Yes. | Yes. |
| Better than Bandwidth? | Sufficient resolution at lower photon energies, not so good at higher ones. | Yes: Resolution as good as the camera allows. |
| Preserves the Photon Beam? | Preserves photon beam for all photon energies. | Starts absorbing too much of the beam below about 4000 eV, depending on thickness of the plates. |

## Attenuator

The gas attenuation is necessary to ensure that the users can dampen the FEL beam's intensity without significantly distorting the wavefront of the photon pulse, and the solid attenuators will be used to reach a level of attenuation that could not be easily achieved with gas alone. The goal is to ensure that the users can enjoy a factor of 1000 attenuation with just the gas over the whole range of the FEL (up to 14,000 eV), and a factor of 10,000 with a combination of the gas and solid attenuators.

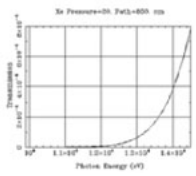

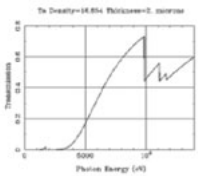

The best gas to be used for the hard x-ray attenuation would be Xe, with pressures going up to 30 mbar to get the factor of 1000 attenuation at the higher photon energies for a 8-m long attenuator. For the solid attenuators, the best materials would be tantalum or tungsten, due to their high density, large cross sections, inertness, and high melting temperatures. The figures above show their transmissions (source: CXRO).

## General Layout Concept

The attenuator needs to be in the middle of the diagnostics, with position, and intensity monitors on both sides to see how the attenuation is affecting the beam. The pulse arrival time and length monitor should be placed as close to the beamline exit flange as possible to give the users the most accurate measurements and avoid arrival time distortions from the optical components in the beamline. The 'destructive' diagnostics would be a set of screens, diodes, and wire scanners that would be put in and out of the beam by the operators for initial adjustments.

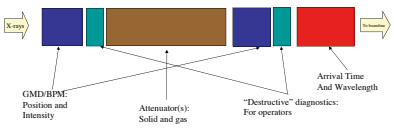


*pavle.juranic@psi.ch

## Poster # 5

# Electronic and Structural Dynamics in Solution: Pump-Probe XAS, XES, RIXS

**Chris J. Milne**
***Laboratoire de Spectroscopie Ultrarapide, EPFL, Lausanne, Switzerland***

### What are we interested in ?

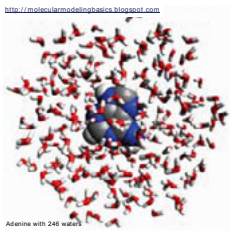


Investigating excited state dynamics of species in solution to try to understand how energy moves in these strongly interacting systems

How does the solvent interaction play a role in the relaxation of these systems ?

How does the excitation perturb the structure and how does this structural change affect the energy transfer and relaxation ?

Can we relate this information to functionality ?

### Current ultrafast x-ray sources at the SLS

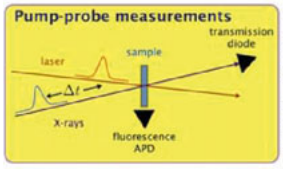


**microXAS beamline**
- tuneable hard x-ray in-vacuum undulator (4-20 keV)
- Si (111), Ge(111) & Si(311) monochromator crystals
- micro-focus capability (< 1μm²)
- $10^{12}$ photons/second

**SuperXAS**
- tuneable from 4.5 to 35 keV
- Si(111) monochromator
- X-ray emission spectrometers available:
5 crystal Johann-type Si(111)
1 crystal Johann-type (range of crystals)
1 crystal von Hamos-type (single-shot)
- $10^{11}$-$10^{12}$ photons/second

**The FEMTO slicing source at microXAS**
- tuneable from 4 to 20 keV
- bandwidth 1%, 0.03%, 0.015%
- 140 ± 30 fs x-ray pulse duration
- timing stability of < 30 fs RMS over days
- $10^3$ photons/second @ 1% BW

**PHOENIX beamline**
- tuneable "tender" x-ray in-vacuum undulator (0.8-8 keV)
- Si (111), KTP, Be, InSb monochromator crystals
- micro-focus capability (< 1μm²)
- $10^{11}$-$10^{12}$ photons/second

### X-ray absorption spectroscopy: Retrieving structural information

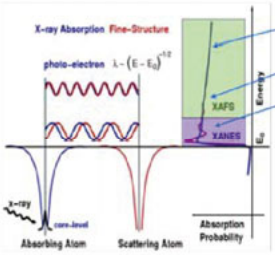


**EXAFS:** distances to neighbouring atoms

**XANES:** oxidation state, geometry, coordination environment

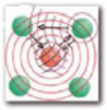

This works in any medium and is element-specific

### X-ray emission spectroscopy: Retrieving electronic information

As with optical spectroscopy you will see all the emission lines if you're above the absorption edge

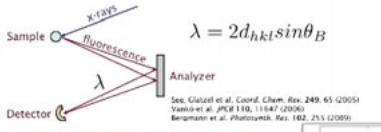


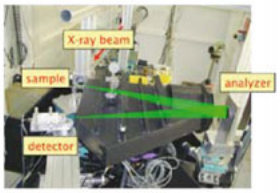


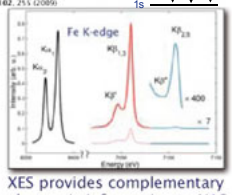


XES provides complementary electronic information to XAS

### Pump-probe XAS/XES at SwissFEL

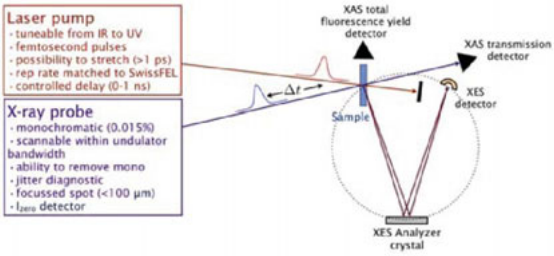


### At the sample x-ray beam parameters

| Parameter | | Unit | Requirement | Motivation / Remarks |
|---|---|---|---|---|
| **Beam parameters** | | | | |
| Energy | | keV | 2-12 keV | determines which elements can be investigated |
| | stability | | 0.01% | ideally less then bandwidth of undulator |
| Bandwidth | | % | 0.01% or better | after monochromator |
| | stability | | <±5% | if the bandwidth of the mono is unstable that's not good |
| Beam position | stability | | <±10% beam FWHM | this is coupled to the pump laser available |
| Beam size | | μm | 20 μm to 500 μm | Gaussian profile ideally |
| Photons per pulse | | #ph | the more the better | also requires possibility to attenuate |
| | stability | | 1% peak-to-peak | or an excellent bzero monitor is required |
| Pulse length | | fs | 5 fs to 10 ps | ability to stretch x-ray pulse lowers peak power |
| | stability | | <10% | |
| Pulse arrival time | stability | fs | < pulse duration | otherwise short pulse duration is worse then useless |
| **Beam parameter changes during experiment** | | | | |
| Energy | range / step | eV | 0.2 eV | more appropriate would be in BW: 0.005% |
| | rate | eV / min | 60 eV/min | for spectroscopy this is a core requirement |
| Beam size (microfocus only) | range / step | μm | --- | not generally required |
| | rate | μm / min | --- | not generally required |
| Pulse length | range / step | | --- | not generally required |
| | rate | | --- | not generally required |
| **Beam geometry** | | | | |
| Beam slope | max. tolerable | μrad | --- | Thin samples make this not an issue |
| Working distance | min. required | mm | >300 mm | Some space is required for laser optics |
| **Other** | | | | |
| | | | | |

### Solvation dynamics: aqueous iodide

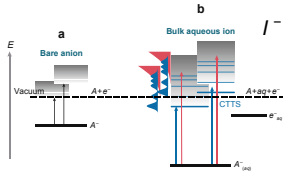


$$I^- + H_2O \xrightarrow[\text{UV}]{h} I^0 + e^- + H_2O$$

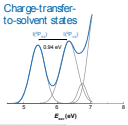


- Chen & Bradforth *ARPC* 59, 203 (2008)
- Pham et al. *JACS* 133, 12740 (2011)

How does the water respond ?

What changes if we excite the CTTS states ?

Can we extract electronic information as well as structural ?

### Myoglobin: Unresolved dynamics & structural issues

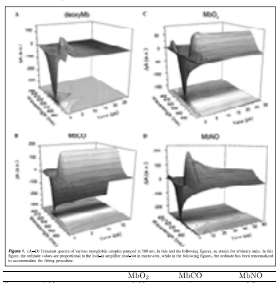


Of the ligands, MbNO is the most interesting but still poorly understood
- NO rebinds very quickly
- Geminate recombination occurs on two timescales (13 & 200 ps)
- There's an indication of a 6-coordinate domed structure S. Kruglik et al. *PNAS* **107**, 13678 (2010)
- MbNO & $MbO_2$ have similar binding geometries but very different affinities
- The geminate recombination has an excitation wavelength-dependence

| | $MbO_2$ | MbCO | MbNO |
|---|---|---|---|
| Quantum yield | 0.28 | 1 | 0.5 |
| Hot 6-coordinate relaxation | 1 ps | - | 1 ps |
| Geminate recombination | 6–5 ps | - | 13 & 200 ps |
| Geminate probability | 0.3 | - | 0.5 & 0.5 |
| Binary recombination | >10 μs | >10 μs | - |
| Binary probability | 0.7 | 1 | - |

X. Ye et al. *JACS* 124, 5914 (2002). E. Scott et al. *J. Biol. Chem.* 276, 5177 (2001)

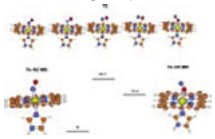

**Figure 2.** Optimized structures for Fe–NO and Fe–ON and the side-on structure (TS). Total energies are given relative to the Fe–NO minimum. Intermediate structures between Fe–NO and TS and TS and Fe–ON along the path are also shown.

D. Nutt et al. *J. Phys. Chem. B* **109**, 21118 (2005)

### Wish List

Jtter < x-ray pulse duration
Sample chamber for anaerobic conditions
Ability to easily scan x-ray energy
multiple crystal von Hamos-type single-shot XES spectrometer
chemical preparation facilities (fume hood, glove box, fridge/freezer sample storage
pixel detectors with a HIGH energy threshold for fluorescence detection


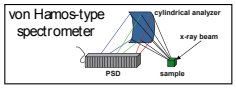


### Acknowledgements

LSU
Frederico Lima
Marco Reinhard
Tom Penfold
Majed Chergui

Hannelore Rittman-Frank
Frank van Mourik
Jochen Rittman

LSU alumni
Wojciech Gawelda
Dimali Amarasinghe
Van-Thai Pham
Andrea Cannizzo

Christian Bressler
Amal El Nahhas
Renske van der Veen
Susanne Karlsson

FEMTO
Steve Johnson
Paul Beaud
Ekaterina Vorobeva
Andrin Caviezel
Gerhard Ingold
Alex Oggenfuss
Simon Mariager
SuperXAS
Maarten Nachtegaal
Jakub Szlachetko

microXAS
Daniel Grolimund
Camelia Borca
Marcus Willimann
Beat Meyer
PHOENIX
Markus Janousch
Thomas Huthwelker
Reto Wetter
SwissFEL
Rafael Abela

**Poster # 6**

PAUL SCHERRER INSTITUT

SwissFEL

# Adaptive gain charge integrating detectors for SwissFEL

A. Mozzanica†, A. Bergamaschi, R. Dinapoli, D. Greiffenberg, B. Henrich,
I. Johnson, D. Maliakal, C. Ruder, B. Schmitt and X. Shi
*Paul Scherrer Institut, 5232 Villigen, CH.*

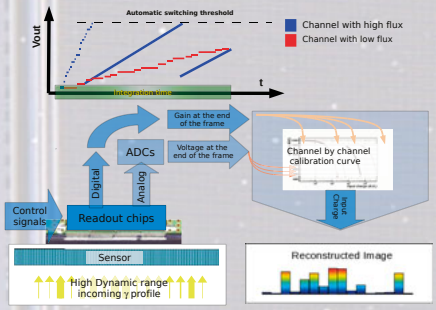


## Automatic gain principle

Before the measurement the amplifier is in reset and the gain is set to high. When the reset is released the charge starts to be integrated on the feedback capacitor. If the output of the amplifier reaches the threshold, a 2nd or 3rd capacitor is switched in, thus lowering the output. At the end of the measurement the analog an gain information are readout.

## Channel Architecture

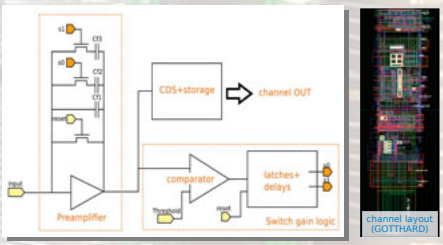


## The GOTTHARD 1D detector

The first strip detector modules with 1280 channels at 50µm pitch have been produced and are now in the commissioning phase. Each module is an independent unit with its own Gigabit link, for fast frame rates (100kHz continuous, 1MHz in bursts) and high scalability. The readout chip has 3 gains in automatic mode plus a fix high gain mode.

## GOTTHARD specifications

| | |
|---|---|
| ASIC technology | IBM 130nm |
| module size | 6.7x12.5cm$^2$ |
| sensitive area | 64x10mm$^2$ |
| sensor thickness | 320-500 µm |
| pitch | 50 µm |
| noise r.m.s. | 160 e.n.c. |
| dynamic range | $10^4$ 12keV photons |
| min Energy | <3.5 keV |
| linearity | better than 0.5% |
| point spread function | O(pitch) |
| min int. time | 80ns |
| dead time | <50ns |
| cooling | air |
| readout time = 1 / frame rate | 100kHz continuos 1MHz burst |

## GOTTHARD test results

Single chip GOTTHARD systems have been tested with X-Ray flourescence light.

- Noise ~160 e.n.c. (r.m.s.) for high gain mode
- Noise ~300 e.n.c. for the 1st gain of gain switching mode
- Noise at low gains ~10 times smaller than Poisson fluctuations
- Gain variation better than 1.5%
- Linearity within 0.5%

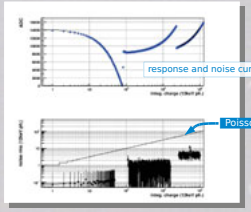


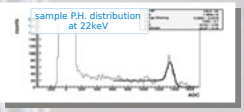


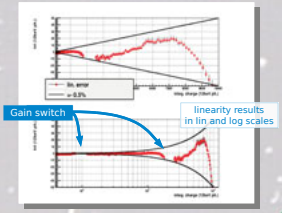


## 2D detector design

- Pixel size 75x75µm$^2$
- ASIC design based on GOTTHARD
- ASIC and module dimension based on EIGER:
  - chip size 1.9x1.9cm$^2$
  - 65kpixel per chip
  - 8 chip per module
  - 0.5 Mpixel per module
- Readout board based on GOTTHARD, with 2 Gigabit links per module.
- Mechanics and cooling based on EIGER

A 4Mpixel detector will be available at first.
Bigger system (9M and 16M) can be requested.

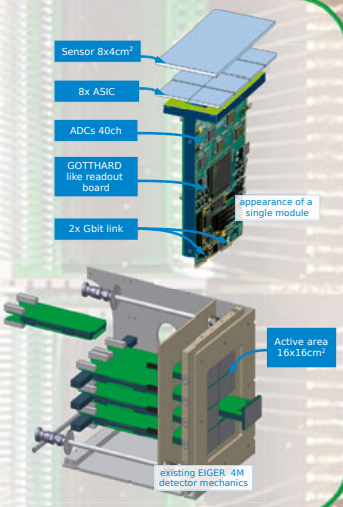


## 2D detector module specifications

The 75µm pixel detector is expected to have marginally better noise and reduced dynamic range with respect to GOTTHARD.
The system will be noise free (i.e. photon counting detector data quality) for photon energies greater than 3-4 keV.
The detector is expected to be available in 2014.

| | |
|---|---|
| ASIC technology | UMC110nm |
| mudule pixel count | 525k |
| mudule size | 80x40 mm$^2$ |
| sensor thickness | 320-500 µm |
| pixel size | 75x75 mm$^2$ |
| dynamic range | up to $10^4$ 12keV photons |
| noise r.m.s. | <150 e.n.c. |
| min Energy | <3 keV |
| linearity | better than 1% |
| point spread function | 1 pixel |
| dead time | <50ns |
| cooling | liquid |
| readout time = 1 / frame rate | 400Hz |

## Options for future 2D detectors

50µm pitch pixel detector:

2 gain stages
automatic gain switching
dynamic range ~2000 12keV photons
active area similar to the 75µm one

25µm pitch pixel detector:

1 gain stage
dynamic range ~200 12keV photons
smaller active area but with similar pixel counts

† *Corresponding author: aldo.mozzanica@psi.ch*

## Poster # 7

# The preliminary optics design of the Aramis undulator beamline of the SwissFEL

*P.Oberta and U. Flechsig*


## Abstract

The X-ray free electron laser at the PSI, the SwissFEL, is a new large facility project. The SwissFEL is planned to be operational in 2016. With a total of three planned undulator beamlines, the SwissFEL will have nine experimental hutches. The authors are presenting a preliminary beamline layout of the first undulator beamline - the Aramis undulator beamline. The Aramis undulator beamline will cover the hard X-ray range from 1.7 keV to 12.4 keV. We had to follow several safety criterions. A common feature for all XFEL designs is a first safety mirror. The mirror distance has to carefully calculated to avoid damage due to high spatial energy densities produced by the SwissFEL. A distance of 50 m was chosen to keep the fluence under 1 eV/atom. We investigated several scenarios. Maximal flexibility and mutual independence of the three experimental hutches was a design priority. Due to the small reflecting angles, the usage of the new designed large offset monochromators (LOM) will be the ground stone for the optical design. Diamond and silicon LOM DCMs are presented. The experimental hutches are equipped with additinal focusing optics, which maked focusing and defocusing optional. To fully exploit the FEL beam properties, the second experimental hutch will receive the raw FEL beam.


### Aramis optics layout

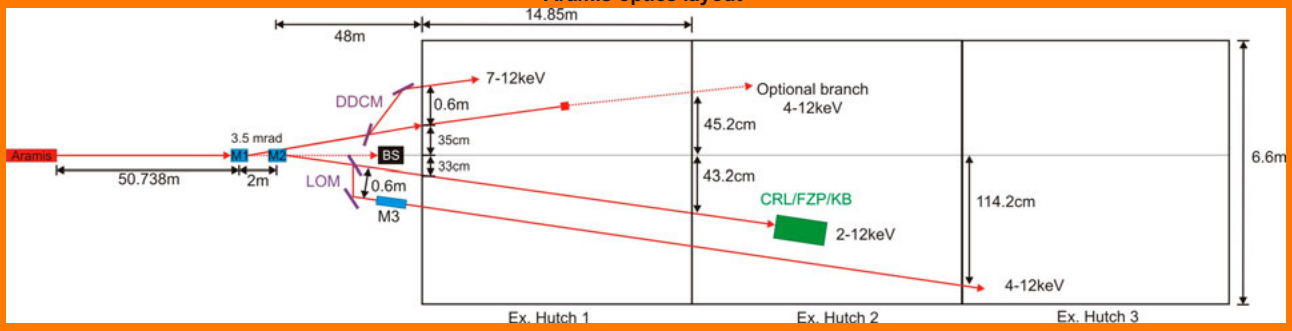


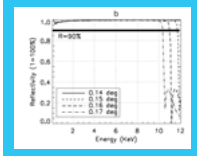

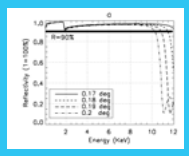

(a) reflectivity plot of an SiC coated mirror substrate at various grazing angles, (b) reflectivity plot of an C coated mirror substrate at various grazing angles.

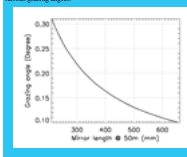

| Parameter | M1 | M2 |
|---|---|---|
| Shape | plane | plane |
| Position (m) | 50 | 53 |
| Geom. surface size (mm) | 375 × 20 | 375 × 20 |
| Bulk material | Si | Si |
| Coating | SiC/C | SiC/C |
| Coating thickness (nm) | 50 | 50 |
| Grazing angle (°) | 0.17/0.14 | 0.17/0.14 |
| Direction of ref. | left | right |

Mirror length versus grazing angle of a mirror placed 50 m behind the Aramis undulator for 4σ acceptance at 7 Å.

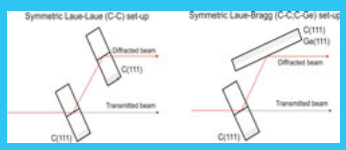


Possible diffraction schemes of the DDCM.

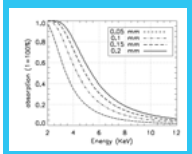

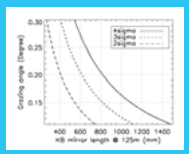

Absorption vs. energy of a diamond crystal with various thicknesses KB length vs. incident angle for three different sigma acceptances at 7 A

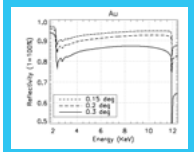

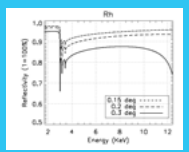

| Parameter | M3 |
|---|---|
| Shape | toroidal |
| Position (m) | 60.925 |
| Geom. surface size (mm) | 400 × 30 |
| Bulk material | Si |
| Coating | Au/Pt/Rh |
| Coating thickness (nm) | 30 |
| Grazing angle (°) | 0.2 |
| Direction of ref. | right |
| r radius (km) | 17.45 |
| ρ radius (m) | 212 |

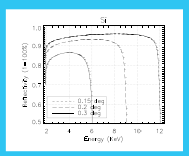

### Experimental Hutch 1

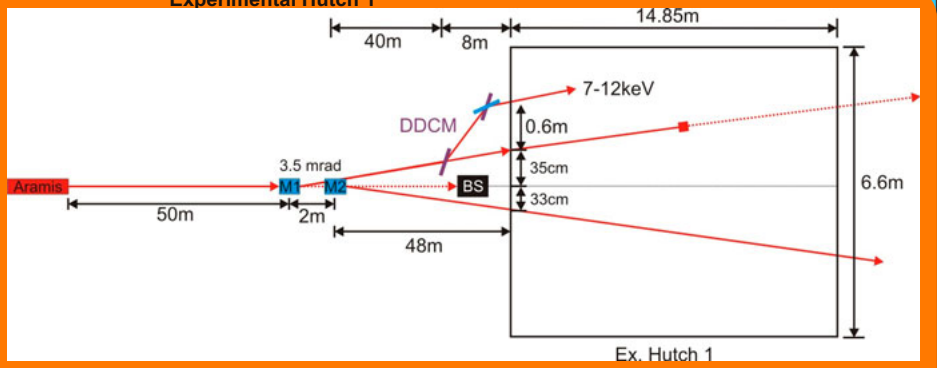


### Experimental Hutch 2

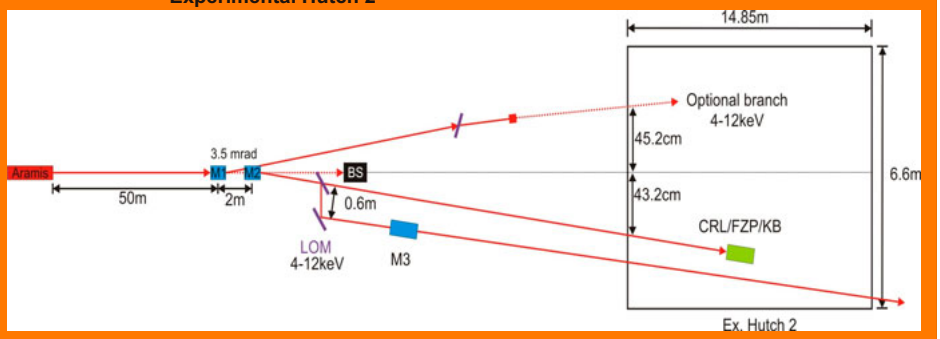


### Experimental Hutch 3

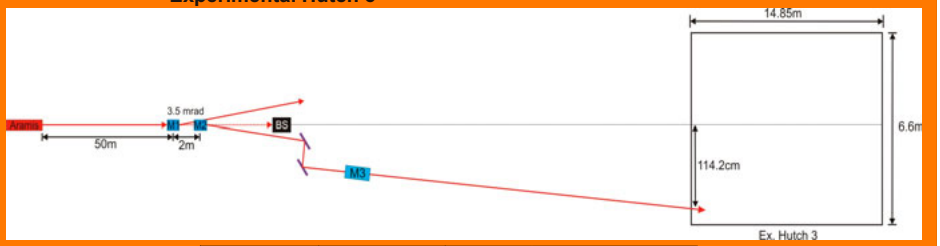


| Exp.hutch | Energy range | E/ΔE | Op. system |
|---|---|---|---|
| 1 | 7 – 12 keV | $6 \times 10^{-5}$ | DDCM |
| 2a | 4 – 12 keV | $6 \times 10^{-2}$ | DDCM |
| 2b | 2 – 12 keV | $1 \times 10^{-2}$ | CRL/FZP/KB |
| 3 | 4 – 12 keV | $< 1 \times 10^{-4}$ | LOM + M3 |

**Poster # 8**

PAUL SCHERRER INSTITUT PSI

# Stimulated Resonant Inelastic X-Ray Scattering

SwissFEL

*Bruce Patterson, Rafael Abela, Bill Pedrini; PSI, 5232 Villigen, Switzerland*

## Introduction

Resonant Inelastic X-ray Scattering (RIXS) is good:
- element specific
- photon-in / photon-out
- may violate dipole-selection rule

*but* it has a very low counting rate.

***Stimulated*** RIXS [1]:
- is analogous to stimulated Raman
- may be orders of magnitude more efficient
- may make t-dependent RIXS possible
- requires high brightness photon beams (XFEL) with multiple $\lambda$

## 1. spontaneous vs. stimulated RIXS

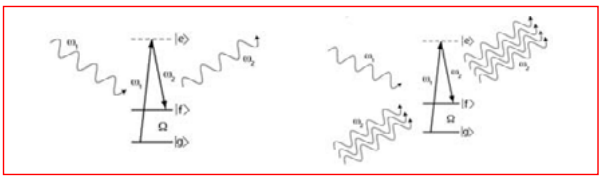

The stimulated cross-sections dominates for an incoming $\omega_2$ φλυξ δενσιτψ

$$F(\omega_2) > \frac{\omega_2^2}{32\pi^3 c^2}$$

This corresponds to only of order $10^9$ ph/XFEL pulse. (LCLS: $10^{12}$ ph/pulse)

## 2. X-ray non-linearity

Stimulated RIXS cross-section is proportional to the 3rd order susceptibility:

$$\frac{d^2\sigma_{stim}}{d\Omega_2 d\omega_2} = \frac{32\pi^2 \hbar\omega_1\omega_2}{\varepsilon_0 c^2} F(\omega_2)\,\mathrm{Im}\left(\chi^{(3)}\right)/N$$

which can be estimated using an anharmonic oscillator model [2]:

$$\chi^{(3)}(\omega_2 = \omega_2 + \omega_1 - \omega_1) = \frac{6Ne^4}{\varepsilon_0 m^3 r_a^2} \frac{\omega_0^2}{\left|\omega_1^2 - \omega_0^2 - 2i\gamma\omega_1\right|^2 \left(\omega_2^2 - \omega_0^2 - 2i\gamma\omega_1\right)^2}$$

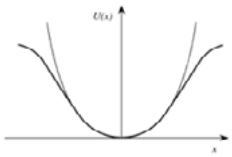

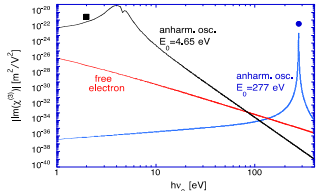


$$\omega_1 = \omega_0 = \omega_2 + \Omega;\ \gamma \approx \Omega << \omega_0;\ \hbar\gamma = 1\,eV$$

$$\chi^{(3)}_{res,X-ray}/N \approx \frac{e^4}{8\varepsilon_0 m^3 r_a^2 \omega_0^2 \gamma^4}$$

## 3. Stimulated RIXS pumping and FWM

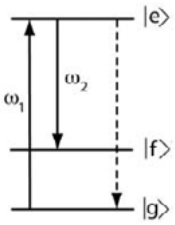


$$\frac{\partial\Delta}{\Delta} \approx \frac{-32\pi I_1 I_2 \tau}{\varepsilon_0 \hbar c^2} \mathrm{Im}\left(\frac{\chi^{(3)}}{N}\right)$$

Stimulated RIXS can be used to efficiently excite an intermediate state $|f\rangle$
This is visible via a decrease in fluorescence (dashed arrow).

For a typical case, full inversion ( $\partial\Delta/\Delta = -1$) occurs for incident peak powers $P_1 = P_2 = 30$ MW. (LCLS: 10 GW!)

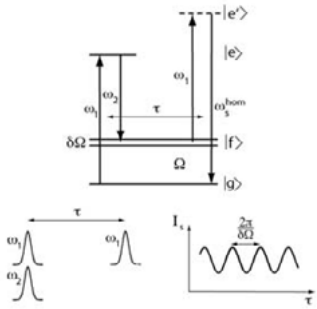


A second stimulated scattering events ( ⇒ "Four-Wave Mixing") can be used to detect coherent quantum beats in the intermediate states.

## 4. Impulsive stimulation

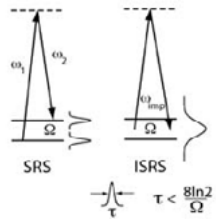


A single broadband pulse (e.g., lifetime broadened) can deliver both the components $\omega_1$ and $\omega_2$.

## 5. SwissFEL possibilities

### A) overcompressed broadband mode

For impulsive stimulation, the pulse bandwidth limits the RIXS excitation energy.

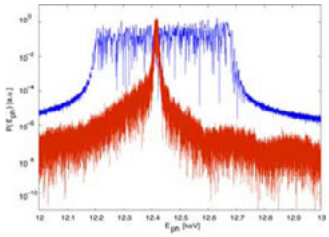

By taking advantage of strong wake fields in the C-band accelerator structures, a 4% FWHM broadband mode is possible (blue curve), i.e., much broader than normal SASE (red) [4]. (LCLS: 1.5%)

### B) 2-color pulses from masked spoiler

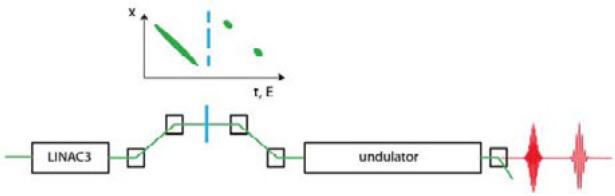


Slits in a thin "spoiler foil" inserted in the LINAC bunch compressor only allow lasing to occur during two temporally-separated slices [5].

Variation of the slit spacing and bunch compressor parameters may allow tuning of the timing and wavelength offsets of the resulting photon pulses [3].

### References

[1] BD Patterson, *SLAC Tech. Note* **SLAC-TN-10-026** (2010)
[2] RW Boyd, *Nonlinear Optics*, Elsevier (2008)
[3] S Reiche, *private communication* (2010)
[4] P Emma, et al, *private communication* (2010)

**Poster # 9**

PAUL SCHERRER INSTITUT PSI

SwissFEL

# Mössbauer Spectroscopic Methods at the SwissFEL

*Bruce Patterson, Rafael Abela, Bill Pedrini; PSI, 5232 Villigen, Switzerland*

## Introduction

So-called "Mössbauer nuclei" have a low-lying, long-lived excited state
- narrow resonance: $\Gamma = \hbar / \tau ; \hbar = 0.66 \text{ eV fs}$
- recoil-less absorption (entire sample carries recoil momentum)
- inelastic spectroscopy (sensitive to magnetism via hyperfine splitting)
- resonant forward scattering (quantum beats)

### Mössbauer nuclei [1]

$^{57}$Fe:
$E_0$ = 14.4125 keV
$\tau$ = 141 ns
$\Gamma$ = 5 neV

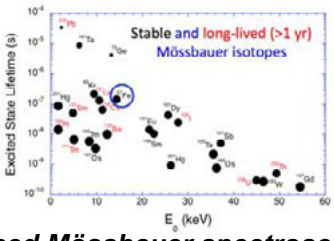


## 1. Synchrotron-based Mössbauer spectroscopy

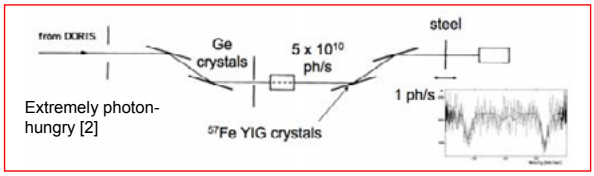


### Highlight: super-radiant Dicke state

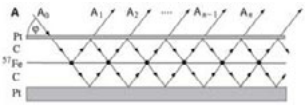

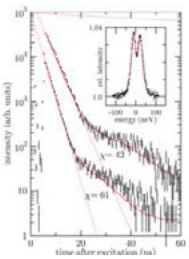

$^{57}$Fe nuclei in a resonant cavity are coherently excited with SR: the super-radiant decay is accelerated by a factor 40-60 [3].

## 2. Advantages of an XFEL

### High resonant flux [4] at 14.4 keV

| | synchrotron | SASE XFEL | seeded XFEL |
|---|---|---|---|
| average flux ph/s/Γ | 2 x 10$^4$ | 3 x 10$^7$ | 3 x 10$^9$ |
| pulse length | 80 ps | 100 fs | 20 fs |
| repetition rate | 5 MHz | 100 Hz | 100 Hz |
| fluence ph/pulse/Γ | 4 x 10$^{-3}$ | 3 x 10$^5$ | 3 x 10$^7$ |

### Background-free pump-probe t-resolved experiments [4]

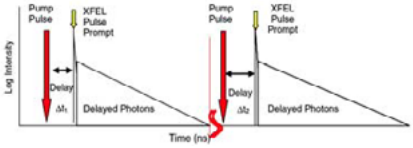


## 3. XFEL Mössbauer ideas

### A) Coherent "filter-foil" spectroscopy [5]

Perform XFEL *S(Q,t)* measurements in the range of ns-ps.

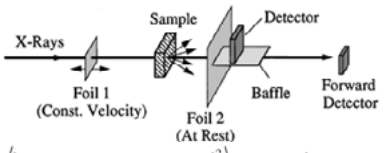


$$I(t) = \left\langle \left| \rho(Q,0)g(t) + g(t)\rho(Q,t) \right|^2 \right\rangle = A + B\left\langle \rho(Q,0)\rho(Q,t) \right\rangle$$

sample(0) foil$_2$(t) — foil$_1$(t) sample(t) — intermediate scattering function S(Q,t)

### B) Active modification of quantum beats [6]

Fast magnetic switching pulse alters hyperfine levels and hence the Mössbauer decay.

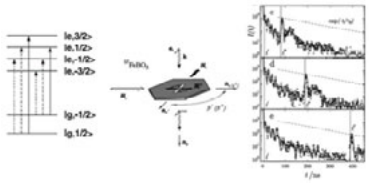

### C) Ultra-high resolution inelastic spectrometer [7]

Polarization filters and rotating Doppler $^{57}$Fe scatterer allow $\mu$eV resolution.

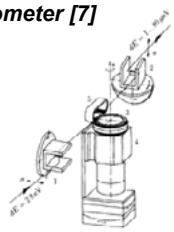

### D) Nuclear Lighthouse Effect [8]

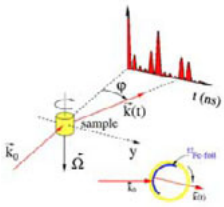


Sample rotation maps time evolution into angle.

## 4. SwissFEL possibilities

### A) 2-photon excitation of $^{57}$Fe [9]

Phase-matching of two 7.2 keV beams in Bragg diffraction allows accurate mapping of $^{57}$Fe in the crystal unit cell.

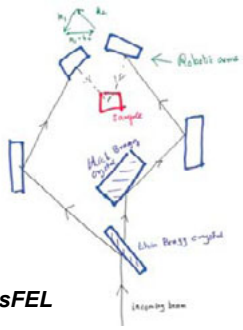

### B) 14.4 keV photons from the SwissFEL

These are foreseen in the extended SwissFEL specifications.

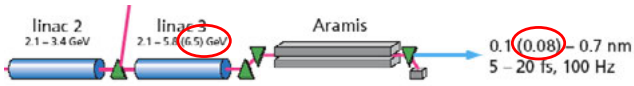


### C) self-seeding seeding at 14.4 keV [10]

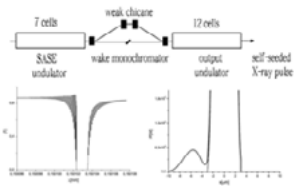

The "stop-band" resonance of a single diamond-crystal monochromator produces a delayed X-ray pulse which can seed a second undulator section.

### References

[1] A Palffy, J. Mod. Optics **55**, 2603 (2008)
[2] E Gerdau, *et al*, PRL **54**, 835, (1985)
[3] R Röhlsberger, *et al*, Science **328**, 1248 (2010)
[4] GK Shenoy and R Röhlsberger, Hyp Int **182**, 157 (2008)
[5] AQR Baron, *et al*, PRL **79**, 2823 (1997)
[6] YV Shvyd'ko, *et al*, PRL **77**, 3232 (1996)
[7] R Röhlsberger, *et al*, NIM Phys Res A **394**, 251 (1997)
[8] R Röhlsberger, *et al*, PRL **84**, 1007 (2000)
[9] S Doniach, *private communication* (2009)
[10] G Geloni, *et al*, arXiv:1006.2045v1 (2010)

**Poster # 10**

PAUL SCHERRER INSTITUT

1 Paul Scherrer Institute, 5232 Villigen, Switzerland
2 Institute of Chemical and Bioengineering, ETH Zurich, Switzerland

# Photocatalytic conversion of $CO_2$ to hydrocarbons over metal doped $TiO_2$: Artificial Photosynthesis

J. Sá[1,2], M. Nachtegaal[1], J. Szlachetko[1], O. Safonova[1] and J.A. van Bokhoven[1,2]

## Background

The increase of atmospheric $CO_2$ to values considered menacing to human life, urged mankind to address the problem. The most sustainable solution is the conversion of $CO_2$ to CO or hydrocarbons, such as methanol:

$$CO_2 + 2H_2O \rightarrow CH_3OH + 1.5O_2 \qquad \text{(Eq. 1)}$$

Such conversion is endothermic, meaning that energy needs to be added for it to take place. The most suitable source of energy is the sun because it is free, clean and abundant. In nature, plants and some bacteria convert $CO_2$ and $H_2O$ effectively into sugars and $O_2$, a process known as photosynthesis. Scientists have for a long time been infatuated with the prospect of performing photosynthesis artificially by means of photocatalysis. Metal-doped $TiO_2$ is able to split water [i] and photoreduce $CO_2$ to CO and hydrocarbons [ii] under UV irradiation ($E_{exitation} \geq$ Eg $TiO_2$ (anatase) = 3.2 eV).

## Objectives of this study

- Determination of electron dynamics
- Determination quantum efficiency of the photocatalytic process

[i] A. Fujishima, K. Honda, Nature 238 (1972) 37.
[ii] S. C. Roy, O. K. Varghese, M. Paulose, C. A. Grimes, ACSNano 4 (2010) 1259.

## Schematic representation of the process:

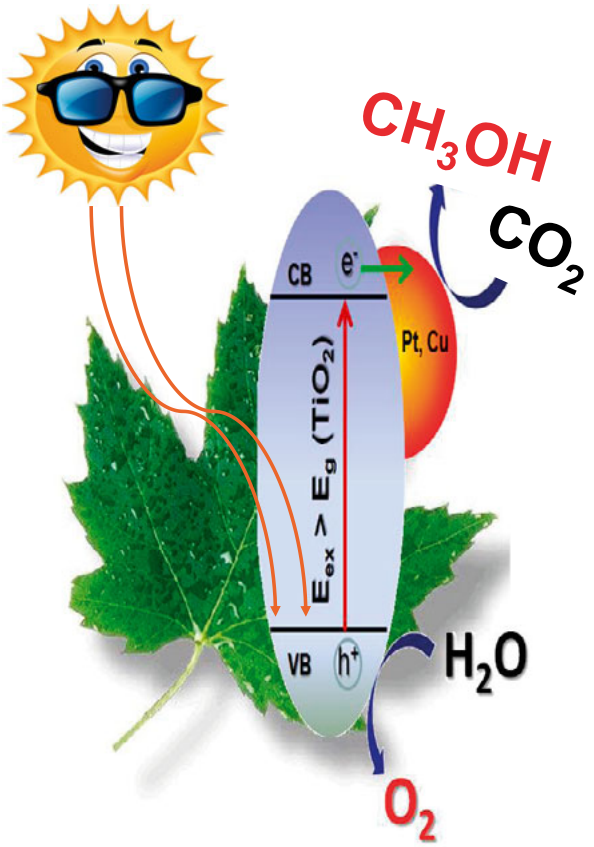


## Proposed experiments:

*Pump-probe for determination of electron transfer yield and time taken for each step*

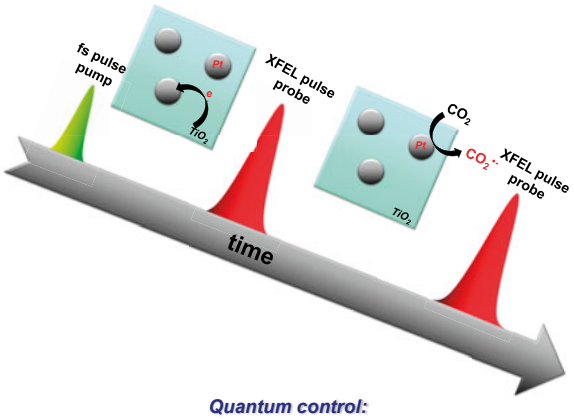


*Quantum control: determination of catalyst state at different surface potentials*

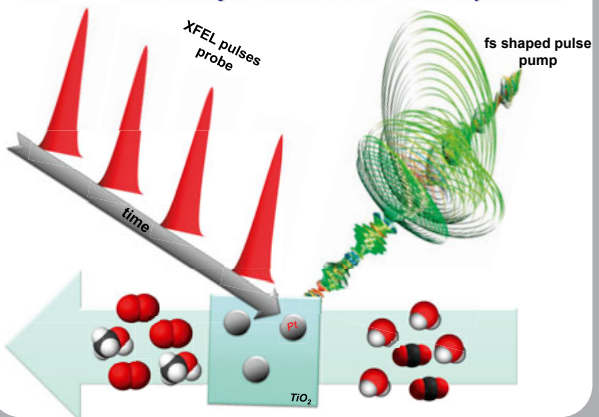


## Remarks

We hope to achieve a fundamental understanding of the photoatalytic process, and thus the development of new materials with better properties, notable enhanced yield. The knowledge can be transfered to other catalytic process in which semicondutors doped with metal are used, since the reactivity is proportional to the net charge transfer [iii].

[iii]( a) X. Ji, A. Zuppero, J. M. Gidwani, G. A. Somorjai, Nano Lett. 5 (2005) 753; (b) J. Y. Park, H. Lee, J. R. Renzas, Y. Zhang, G. A. Somorjai, Nano Lett. 8 (2008) 2388.

**Poster # 11**

PAUL SCHERRER INSTITUT

1 Paul Scherrer Institute, 5232 Villigen, Switzerland
2 University of Fribourg, Switzrland
3 Institute of Chemical and Bioengineering, ETH Zurich, Switzerland

# Single-shot X-ray emission spectroscopy

Jakub Szlachetko[1], Maarten Nachtegaal[1], Jacinto Sá[1],Jean-Claude Dousse[2], Joanna Hoszowska[2], Markus Janousch[1], Olga V. Safonova[1], Anna Bergamaschi[1], Bernd Schmitt[1], Erich De Boni[1] and Jeroen A. van Bokhoven[1,3]

## Background

**The femto second x-ray pulses provided by the free electron lasers requires an spectroscopic instrument able to collect the x-ray fluorescence from the sample within a single shot. The von Hamos spectrometer meets those criteria. The spectrometer geometry results in a scanning-free arrangement thanks to the combination of a cylindrically bent crystal and a position-sensitive detector.**

**Key points:**
- **single shot x-ray emission spectroscopy**
- **energy resolution ~eV**
- **energy bandwidth of 100eV to 500eV**
- **does not require $I_0$ correction**
- **no need for monochromatic beam**

**The von Hamos geometry**

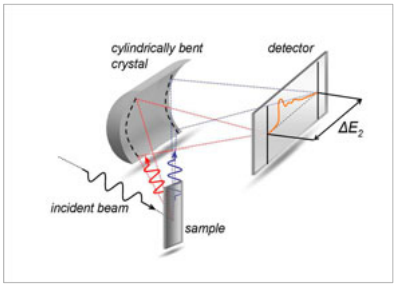


## Experimental

### The von Hamos @ SuperXAS of SLS

**The spectrometer will consist of three diffraction crystals that focus x-ray fluorescence onto the stripe-type MYTHENII detector. To cover x-ray energy range between 4.5keV to 16keV a Ge(100), (110) and (111) cylindrically bent crystals will be used. The energy resolution of the instrument is far below the natural life time broadening of K- and L- core holes.**

**Spectrometer design**

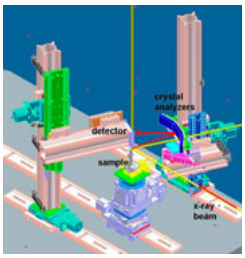


**Crystals for x-ray diffraction**

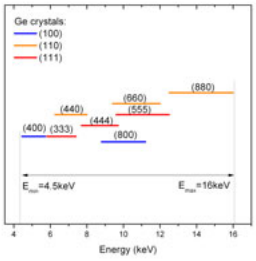


**Spectrometer resolution**

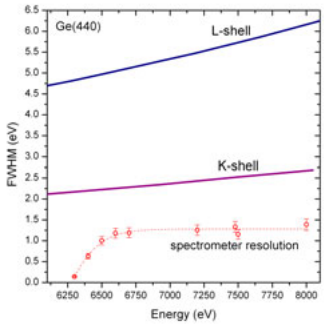


## Proposed experiments

### Study of non-linear absorption mechanism with intense, femtosecond pulses by XES

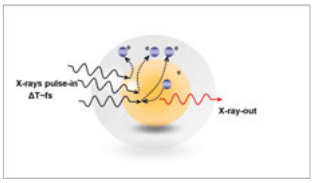


**Cu 2p-1s transition for dose of $1x10^{11}$ photons**

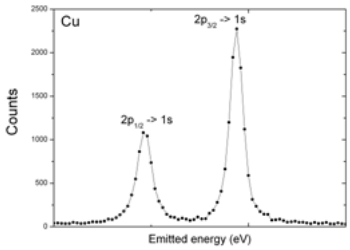


**Occupied electronic states by valence-to-core emission**

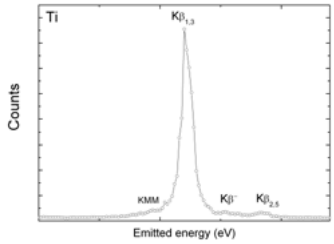


## Conclusions

**The intense and short x-ray pulses delivered by XFEL source provides possibility to study multi-electron excitations in atoms and molecules. The non-linear absorption mechanism, electron relaxation and rearrangement processes can be probed at the femto second time scales. The time dependent evolution of occupied and unoccupied electronic states will give understanding in electron-electron interactions of many-body systems .**

**Poster # 12**

# Constrained optimisation methods for the retrieval of structural information in electron crystallography with limited tilt angles

**Raphael Thierry**[1], Bryant Gipson[2], Henning Stahlberg[1]

[1] Center for Cellular Imaging and Nano Analytics (C-CINA), Biozentrum, University Basel, WRO-1058, Mattenstrasse 26, CH-4058 Basel, Switzerland
[2] Department of Computer Sciences, Duncan Hall, Rice University, Houston, TX 77030, USA

**Abstract** : Electron crystallography uses transmission electron microscopy (TEM) to determine the atomic structure of membrane proteins that exhibit preferential formation in two-dimensional crystals. For geometric reasons, data collection on tilted 2D crystals is limited to ~70º tilt, but for technical reasons the efficiency of data collection at tilt angles higher than 45º is low. Together with noisy data, the problem of three-dimensional reconstruction in electron crystallography is severely ill-posed and needs additional information to reduce the search space of solutions. The reconstruction is usually realized in the Fourier space, where the projected views, once averaged and corrected for the microscope's contrast transfer function (CTF), are merged. The tilt angle limitation results in zero information about the amplitude and phase values in a so-called "missing cone" of the Fourier domain. We present here two novel iterative reconstruction techniques combining projections onto convex/non convex sets (POCS) and mixed constraints, such as density support, positivity, maximal intensity and frequency achievable. The first presented method is an iterative Fienup-Gerchberg-Saxton algorithm that realizes the POCS, while enforcing the boundary and frequency constraints, respectively in the real space and in the Fourier space. The second method recently emerged from the compressed sensing (CS) field, and optimizes separately the reliability to the data (unconstrained tomographic reconstruction) and sparsity cost functions in an alternative manner. The total-variation (TV) norm is chosen as cost function in order to encourage the convergence to solutions having smooth gradient. Each step of the optimization contributes to a convergence to the lowest possible raw data residue, while keeping cost functions at low values. The first method has been tested on an experimental data set of the Bacteriorhodopsin[1], showing full recovery of the missing cone data also from 45º-tilt-angle limited datasets. Both method are general and can be adapted to any tomographic reconstruction problem, i.e for electron crystallography, single particle and for electron tomography on larger biological samples.

## Spaces used in Projective Constraint Optimization (PCO)

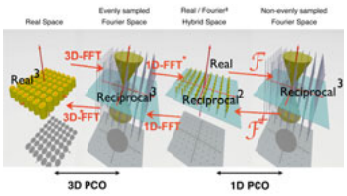


Four different spaces are used :

**Left**: The real space contains the protein structure.

**Mid-left**: The evenly sampled Fourier space contains reciprocal lattice lines.

**Mid-right**: A hybrid space was defined, where real-space representations of lattice line data are located in their reciprocal X/Y Fourier positions.

**Right**: The experimental 3D Fourier space contains the non-evenly sampled experimental measurements along the reciprocal lattice lines. The developed algorithm performed a one-dimensional PCO processing between the non-evenly sampled 3D Fourier space (right) and the Real/Fourier2 hybrid space (mid-right), operating on one lattice line at a time. The three-dimensional PCO performed a refinement between the real 3D space (left) and the evenly sampled Fourier space (mid-left).

*All Illustration for PCO method were taken from [1].*

## Cylindrical Ring Correlation analysis

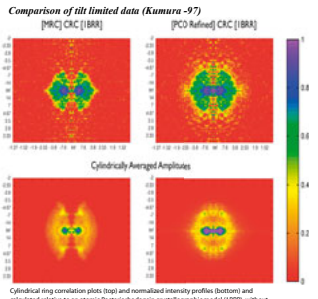


Cylindrical ring correlation plots (top) and normalized intensity profiles (bottom) and calculated relative to an atomic Bacteriorhodopsin crystallographic model (1BRR), without (left column) and with (right column) refinement by the here described PCO refinement algorithm. Plots are given as a function of ring of radius ρ (horizontal axis, in Å), and height z (in the vertical axis, in Å ) in Fourier space.

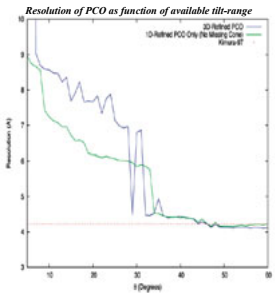


The average resolution is estimated by Fourier shell correlation (FSC, 0.5 threshold) with the 1BBR model. The original MRC reconstruction was based on data up to 60° specimen tilt, and showed a 4.4 Å res. The plot shows that a tilt limitation to only ± 10°sample tilts still allows a 9 Å reconstruction. Inclusion of data up to only 35° tilts effectively allowed the full reconstruction of the structure up to a resolution of 4.5 Å . Inclusion of data beyond a 45° tilt range did not bring any further improvements.

## Structural Comparison

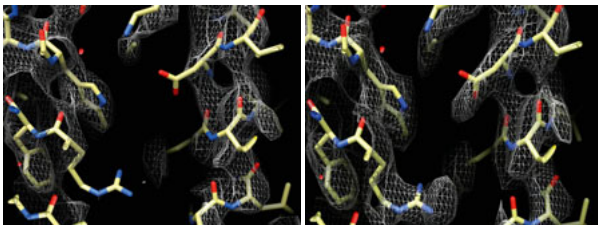

An area from the transmembrane part of the Bacteriorhodopsin monomer close to the Schiffbase, shown before (left) and after (right) the iterative refinement by PCO. The grid surrounds the reconstructed volume. The atomic model of an XRD-determined structure of BR (PDB: 1BRR, Essen et al., 1998) is shown for comparison only. A first 100 rounds of PCO were applied, followed by 30 further rounds including edge detection and sharpening as additional masking constraints. After refinement with PCO, the wrong connections in the alpha-helical backbone of the electron density map are corrected, and side-chain densities were generated.

## Constrained convex optimization from the compressed sensing view

The method seeks to minimize the total variation norm (TV-norm) of the image

$$\vec{f}^{\,*} = \arg\min \left\| \vec{f} \right\|_{TV} = \arg\min \left( \sum_{i,j,k} \sqrt{\left(f_{i,j,k} - f_{i-1,j,k}\right)^2 + \left(f_{i,j,k} - f_{i,j-1,k}\right)^2 + \left(f_{i,j,k} - f_{i,j,k-1}\right)^2} \right)$$

subject to the convex constraints in $C$

$$C : \begin{cases} \left| P\vec{f} - \vec{g}_{data} \right| \le \varepsilon_d & (1) : \textit{reliability to measures} \\ \vec{f} \ge 0 & (2) : \textit{positivity} \\ \vec{f}\left(x \in NullSup\right) = 0 & (3) : \textit{Zero Mask} \end{cases}$$

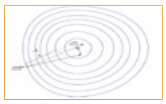

*Adaptation of the Gradient step size. The new image iterate is a linear combination of the POCS optimisation and the TV minimization. The scalar λ is chosen so as to ensure a monotonic decrease of the data residual . Illustration taken from [2].*

## Acceleration of Projector/Backprojector in POCS with NUFFT

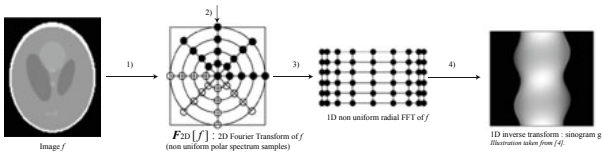


Basic steps of a 2D-NUFFT forward projection in parellel-beam CT.

1) 2D- NUFFT of image $f$ to obtain polar spectrum samples on regular polar sample space
2) Multiply radially by the frequency response of the effective detector blur.
3) One-dimensional NUFFTs along radial direction r for each angle θ.
4) One-dimensional Inverse transform to get the sinogram g = R$_\theta f$ = $\boldsymbol{F}_{1D}$ (Projected image)

## Comparison of reconstruction algorithm performance on a 2d-slice of a X-ray model of Chaperonin-group II

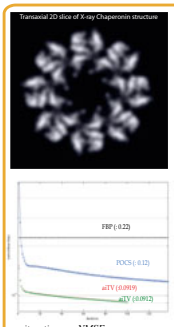


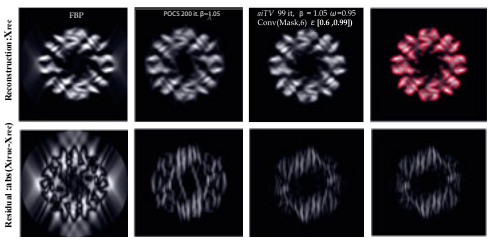


120 projections acquired on [-60,60]-degree angular orbit, corrupted with Poisson noise (λ~325) were generated

References:
[1] B.Gipson et al, Phys. Rev E 84,011916 (2011)
[2] L.Ritschl et al, Phys. Med. Biol. 56 (2011) 1545-1561
[3] Y. Kumura et al, Nature (1997)
[4] Y. O' Connor et al, IEEE Trans Med Ima. 25, vol 5 (2006)

UNI BASEL

BIOZENTRUM Universität Basel The Center for Molecular Life Sciences

STRUCTURAL BIOLOGY National Center of Competence in Research

CINA - part of SystemsX The Swiss Initiative for Systems biology

## Poster # 13

# Multidimensional high energy experiments with X-rays and electron pulses.

F. Carbone

[1] Laboratory for Ultrafast Microscopy and Electron Scattering (LUMES), ICMP, Ecole Polytechnique Fédérale de Lausanne, CH-1015 Lausanne, CH

ÉCOLE POLYTECHNIQUE FÉDÉRALE DE LAUSANNE

LUMES

### Motivation: Comparison between electons and X-ray sources for diffraction:

| | X-FEL | 10 KV e⁻ | 100 KV e⁻ | 1 MV e⁻ |
|---|---|---|---|---|
| Pulse duration | 1 fs | 500 fs - 1 ps | 50-500 fs | 1-30 fs |
| Particles per pulse | $10^{13}$ | $10^{2}$ - $10^{4}$ | $10^{4}$ -$10^{6}$ | $10^{6}$ - $10^{8}$ |
| Cross section (barns) | 1-10 | $10^{7}$ | $10^{6}$ | $5*10^{5}$ |
| Relative spatial Coherence length $L_t/D$ | 0.1-0.2 (full coherence = 1) | $10^{-5}$ ($10^{3}$ e⁻) | $10^{-4}$ ($10^{6}$ e⁻) | $10^{-2}$ – $10^{-3}$ ($5x10^{6}$ e⁻) |
| Spatial resolution | 0.1 nm | pm (diffraction) | 0.2 nm (image) pm (diffr.) | 0.05 nm (image) pm (diffr.) |
| Particles per image (100x100 nm, 2 A res.) | $10^{12}$ | $10^{6}$ | $10^{6}$ | $5*10^{6}$ |
| Radiation dose per image Gy | $10^{7}$ Gy | $5*10^{6}$ Gy | $5*10^{6}$ Gy | $10^{7}$ Gy |
| Probe depth | ~ 100 μm | 10-50 nm | 50-200 nm | 200-500 nm |

A perspective on novel sources of ultrashort electron and X-ray pulses
F. Carbone , P. Musumeci , O.J. Luiten , C. Hebert. Chemical Physics (2011)

### Electron diffraction set-ups (probe):

10-50 KV, Reflection/transmission Geometry, stroboscopic, ~ 100 fs resolution

G. Mancini et al, in preparation

100 KV, Transmission geometry. $10^{6}$ e⁻/pulse, ~ 60 fs resolution. single shot per time delay.

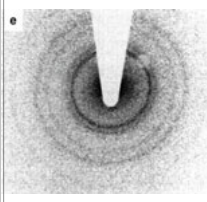

T. van Oudheusden et al., Phys. Rev. Lett. 105 (2008) 264801.

MV, Transmission geometry. $10^{8}$ e⁻/pulse, ~ 50 fs resolution. single shot all transient.

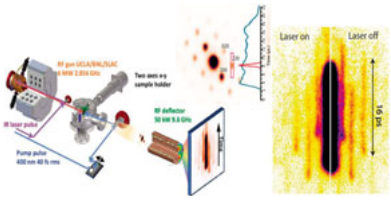


P. Musumeci et al., J. Appl. Phys. 108 (2010) 114513

### Excitation with photons: pump

Electron-hole pair excitation

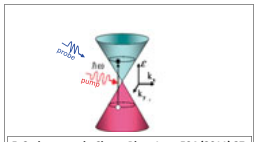

F. Carbone et al., Chem. Phys. Lett. 504 (2011) 37

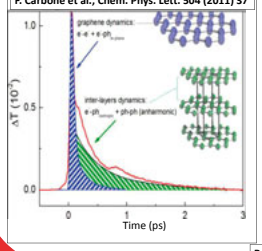


Temperature jump

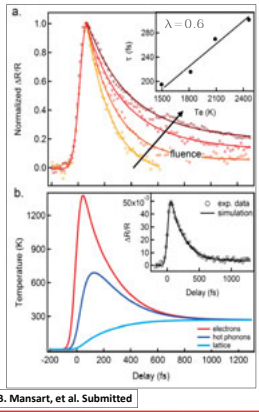


B. Mansart, et al. Submitted

THz excitation

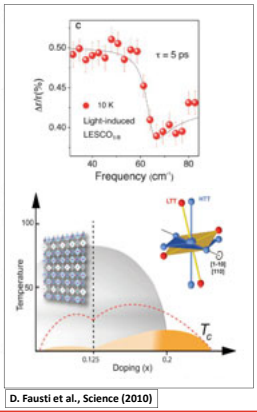


D. Fausti et al., Science (2010)

Raman excitation

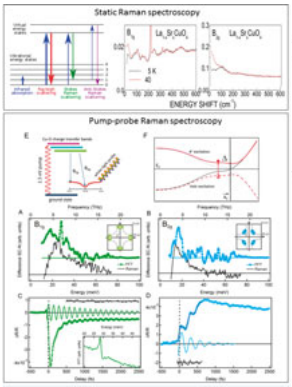


B. Mansart, in preparation

High energy Raman processes

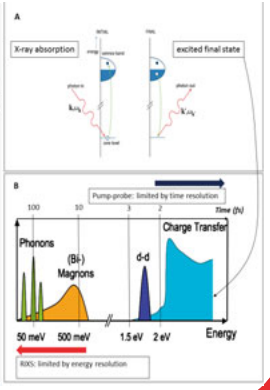


### X-ray/electrons pump-probe experiments

High energy electron diffraction, imaging, spectroscopy

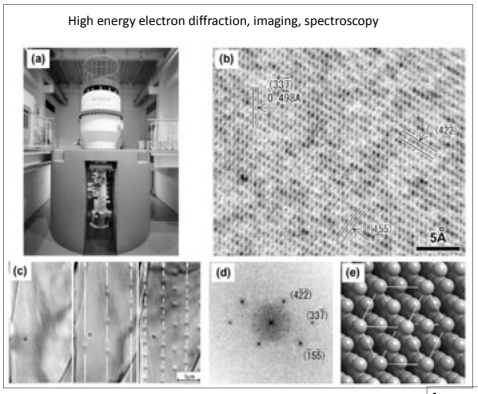

- Multidimensional high energy spectroscopy
- Chemically selective photodoping
- Magnetic imaging
- Diffraction

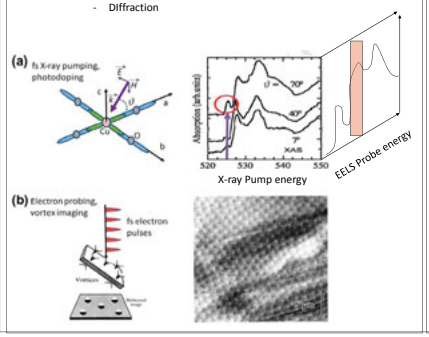


Single shot protein imaging and radiation damage

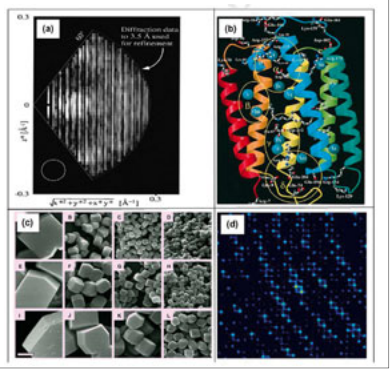

A perspective on novel sources of ultrashort electron and X-ray pulses
F. Carbone , P. Musumeci , O.J. Luiten , C. Hebert. Chemical Physics (2011), and references therein

### Propositions:

Technically:
- Realize a beamline for high-energy electron diffraction, imaging and spectroscopy
- Make it possible to interface such an instrument with advanced photon sources.
- Create a «critical mass» laboratory for ultrafast science capable of accessing different excitations energies

Scientifically:
- These tools provide a unique way of observing phase transitions in solids, liquids, gases and aggregates
- High energy electrons have enhanced contrast to magnetism via Lorentz microscopy
- Radiation damage can be studied in hybrid single shot experiments using electrons, X-rays or ion beams

**Poster # 14**

# Ultrafast anisotropic X-ray scattering in the condensed phase

T.J. Penfold, I. Tavernelli, R. Abela and M. Chergui.
thomas.penfold@epfl.ch and majed.chergui@epfl.ch

ÉCOLE POLYTECHNIQUE FÉDÉRALE DE LAUSANNE

PAUL SCHERRER INSTITUT

## Problem

The advent of X-ray free electron lasers offers new opportunities for X-ray scattering studies of the ultrafast molecular dynamics in liquids, which was so far limited to the 100 ps resolution of synchrotrons. Photoselection induces anisotropy in the sample, which enhances the contrast of the signal from excited molecules against the diffuse background, while allowing probing of their vibrational and rotational dynamics. Here, we present a computational approach for calculating the transient scattering intensities of iodine in n-hexane, based on molecular dynamics simulations. We also derive, using realistic parameters the anticipated signal-to-noise ratio for a large class of diatomic elements in solution.

## Basic Concept

The use of polarised pump laser pulses induces an anisotropy of the sample by preferably photoexciting those molecules that have a favourable orientation of their transition dipole moment with respect to the electric field vector of the laser [4]. Subtracting the unexcited sample pattern will therefore leave the contribution from the excited molecules, i.e. the anisotropic component and therefore were unable to fully characterise the signatures of vibrational and reorientational dynamics.

## In the Future

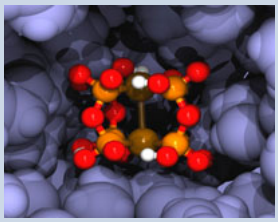

Bimetallic complexes, such as $[Pt_2(POP)_4]^{4-}$ ($POP = [H_2P_2O_5]^{2-}$) would be highly suited to fs XRS. This complex exhibits a rich wavepacket dynamics along the Pt-Pt bond, identical to that of a diatomic molecule [6].
This work is a first step in the investigation of fs XRS and further work to include solvent induced non-adiabatic processes and rotational diffusion is underway.

## References

[1] TJ Penfold *et al.*, *PRL*, *submitted*.
[2] M Chergui and AH Zewail, *Chemphyschem*, **10**, 28 (2009).
[3] M Chergui, *Acta Cryst A*, **66**, 229 (2010).
[4] JP Bergsma *et al.*, *J Chem Phys*, **84**, 6151 (1986).
[5] B Hess, C Kutzner, D van der Spoel, and E Lindahl. *JCTC*, **4**, 435 (2008).
[6] RM van der Veen *et al.*, *J Am Chem Soc*, **133**, 305 (2011).

## Acknowledgements

The authors thank Bruce Patterson for useful discussions and Ursula Rothlisberger for computational resources. This work was partly funded by the NCCR MUST network.

## The Transient Patterns and Signal to Noise Ratio

The calculation of anisotropic scattering signals is computationally expensive for liquid solutions where a large number of atoms must be considered. However anisotropy will only be introduced via the excited solute and a small region of the solvent in close proximity. Therefore, by solving exactly for the solute and a small region of the solvent around it, we can obtain realistic signals at much reduced computational expense:

$$\tilde{I}(\mathbf{q}) = \sum_h f_h^2(\mathbf{q}) + \sum_{j\neq h} f_h(\mathbf{q}) f_j(\mathbf{q}) \exp^{-i\mathbf{q}r_{hj}} + \sum_k N_k f_k^2(\mathbf{q}) + N_k N_l V \sum_{l\neq k} f_k(\mathbf{q}) f_l(\mathbf{q}) \int_{-\infty}^{\infty} (g_{kl}(r) - 1)\sin(\mathbf{q}r)\mathbf{q}r 4\pi r^2 dr \quad (1)$$

The intensity can be calculated from snapshots of molecular dynamics (MD) simulations of excited molecular systems. Below we plot the transient scattering patterns, with an without the solvent in the anisotropic region.

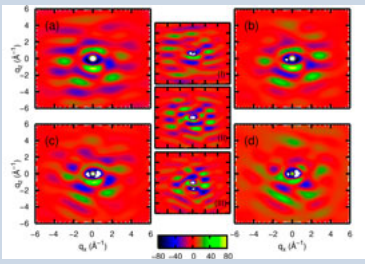

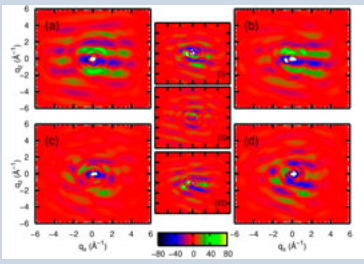

Given that these simulations concern only 3000 configurations, they hold the promise that single shot XRS of solutions can be envisioned at X-FELs. Therefore, we use realistic X-FEL parameters to predict a signal to noise ratio (S/N) for planning future experiments. The derived S/N as a function of element and photolysis yield indicates that from a single shot X-ray diffraction experiment it would be possible to obtain a S/N$\geq$ 1 for a photolysis yield of 3% from the elements heavier than iron. For the heaviest elements (ruthenium, iodine and platinum) the S/N can be greater than 3 and therefore one could expect a good experimental contrast.

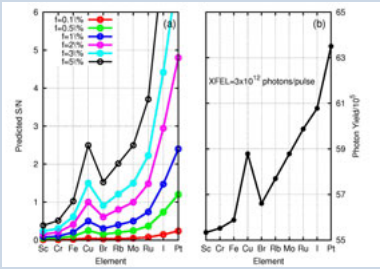

We note that intensity fluctuations in the X-ray intensity would lead to a reduction in the signal to noise ratio. This could make single shot experiments for the lighter elements very difficult. In such cases accumulation could be used. This requires the accurate knowledge of the incoming X-ray intensity to account for shot to shot fluctuations. This can be measured to less than 0.5% as demonstrated in running experiments at the LCLS Facility (Stanford) and therefore we do not expect this to be a limiting factor.

## Computational Details

The MD simulations were performed with the GROMACS molecular dynamics package [5].The system is composed of one $I_2$ molecule and 106 hexane molecules within a box of 28 $Å^3$. It was propagated in the ground state for 20 ns, from which 3000 configurations from the last 5 ns were selected randomly and used.

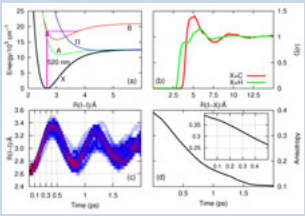

100 out of the 3000 configurations were selected for the excited state dynamics according to the alignment of the transition dipole of $I_2$ with the electric field of the pump laser. These configurations were then propagated for 2 ps and snapshots from the photoselected simulations were taken at 100, 200, 300 and 400 fs. We assume an X-ray probe pulse at 8 keV with a 0.1% bandwidth and a temporal width of 10 fs.

**Poster # 15**

PAUL SCHERRER INSTITUT PSI

must | Molecular Ultrafast Science And Technology

National Center of Competence In Research

# Ultrafast Structural Dynamics in Strongly Correlated Electron Systems: Timing Specifications

Andrin Caviezel, Paul Beaud, Simon Mariager, Sebastian Grübel, Jeremy Johnson, Gerhard Ingold
*FEMTO Group, Laboratory for Synchrotron Radiation – Condensed Matter, Paul Scherrer Institut, CH-5232 Villigen, Switzerland*

*Urs Staub*
*RESOXS Group, Laboratory for Synchrotron Radiation – Condensed Matter, Paul Scherrer Institut, CH-5232 Villigen, Switzerland*

Steve Johnson
*Physics Department, Swiss Federal Institute of Technology (ETH), CH-8093 Zürich, Switzerland*

## Science

**Goal:** Understand complex interactions between lattice and electronic degrees of freedom in strongly correlated electron systems which often lead to exotic electronic and magnetic properties, *such as High-Tc superconductivity, colossal magnetoresistance, multiferroicity, ...*

Experiments at FEMTO on a manganite [1] and on a charge density wave system [2] demonstrated that photo-doping can induce non-thermal phase transitions as evidenced by the disappearance of a superlattice reflection. Initial dynamics are significantly faster than the FEMTO time resolution of 200 fs. Optical data on a magneto-resistive manganite indicate [3] relevant dynamics up to 30 THz.

To resolve these dynamics in greater detail and to disentangle the atomic motions within the unit cell requires measurement of as many Bragg reflections as possible with sufficient time resolution. Only an FEL can provide the required time resolution of < 20 fs with sufficient flux to efficiently measure the relevant but often weak superlattice peaks.

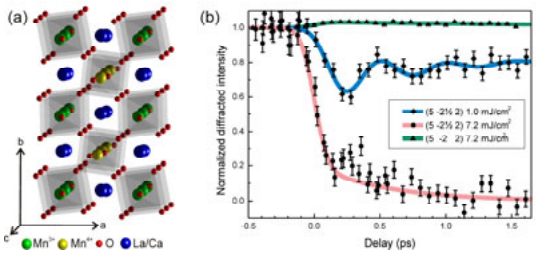


## Diffraction setup

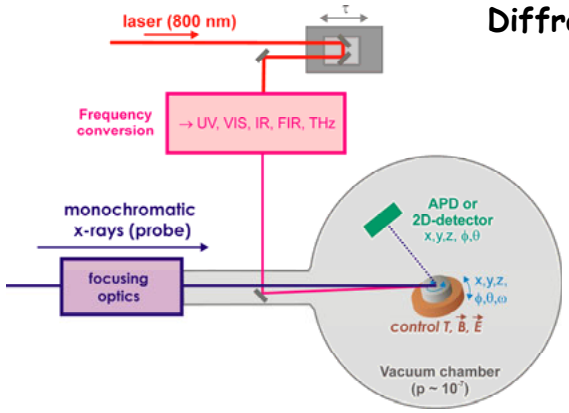


**Sample environment:**
Temperature: 5 – 500 K
Static magnetic field: 0 - 10 T
Static electric field: 0 – 5 kV

**Matching X-ray probe depth to excitation depth (often < 50 nm):**
- solution 1: use thin films
- solution 2: use grazing incidence diffraction to match probe to excitation depth, requires severe focusing of incoming x-rays in the plane of incidence [4].

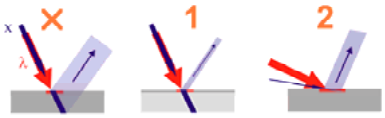


## Requirements at SwissFEL for pump-probe diffraction experiments

### X-rays

| Parameter | | Unit | Requirement | Motivation /Remarks |
|---|---|---|---|---|
| Energy | | keV | 2 – 12 | High q-space coverage; select edges for resonant diffraction |
| | stability | % | 0.002 | Monochromator required |
| Bandwidth | | % | 0.002 | Monochromator required |
| | stability | % bw | < 10 | |
| Beam position | stability | µm | < 1 | |
| Beam size | | µm | 1 – 100 | Grazing incidence requires ~1 µm focus (horizontal dimension only) |
| Photons per pulse | | | $10^8 – 10^{12}$ | Attenuator needed to avoid sample damage |
| | stability | | - | Shot-to-shot normalization with $I_0$ |
| Pulse length | | fs (rms) | 2 | Short pulse mode |
| | stability | % | 10 | |
| Pulse arrival time | stability | fs (rms) | < 5 | With respect to pump laser |
| **Beam parameter changes during experiment** | | | | |
| Energy | range | eV | ±100 | Required for resonant diffraction |
| | step | eV | | Required for resonant diffraction |
| | scan | eV / sec | 0.2 | Required for resonant diffraction |
| Beam size | | | - | Only adjusted during setup |
| Pulse length | | | - | Only adjusted during setup |
| **Beam geometry** | | | | |
| Beam slope | maximum | µrad | 200 | |
| Working distance | minimum | mm | 500 | UHV vacuum chamber; sample rotation, translation, cooling |

### Diagnostics

| Parameter | Resolution | Range | Single shot |
|---|---|---|---|
| Intensity | $10^{-3}$ | 0 - $10^{12}$ ph | yes (after monochromator) |
| Beam position | 1 µm | ± 100 µm | yes |
| Beam width | 5 um | 0 - 300 µm | yes |
| Pulse duration (rms) | 1 fs | 0 - 200 fs | nice to have |
| Arrival time, coarse (rms) | 200 fs | ± 500 ps | yes |
| Arrival time, fine (rms) | 2 fs | ± 500 fs | yes |
| Mean energy | $10^{-3}$ | | no (since mono is used) |
| Energy spectral width | $10^{-3}$ | | no (since mono is used) |
| Longitudinal source point | 1 m | ± 20 m | no |

### Excitation pulse (derived from laser or THz accelerator)

| Parameter | | Unit | Requirement | Motivation /Remarks |
|---|---|---|---|---|
| Optical | wavelength | µm | 0.25 – 2 | |
| | pulse width | fs (FWHM) | < 20 | Pulse shaping, multiple pump pulses |
| | jitter | fs (rms) | < 5 | With respect to x-ray pulses |
| Far IR / THz multi cycle pulses | wavelength | µm (THz | 15 – 150 | |
| | pulse width | fs (FWHM) | 500 – 20000 | Amplitude phase stable |
| | jitter | fs (rms)<br>% cycle period | 5<br>10 | Whichever is larger |
| | energy/pulse | µJ | > 10 | |
| THz half cycle | frequency | THz | 0.1 – 10 | |
| | field strength | MV / cm | 0.1 – 10 | |

[1] P. Beaud S. L. Johnson, E. Vorobeva, U. Staub, R. A. De Souza, C. J. Milne, Q. X. Jia, and G. Ingold, *Phys. Rev. Lett.* **103**, 155702 (2009)
[2] E. Möhr-Vorobeva, S. L. Johnson, P. Beaud, U. Staub, R. De Souza, C. Milne, G. Ingold, J. Demsar, H. Schaefer, A. Titov, *Phys. Rev. Lett.* **107**, 036403 (2011)
[3] D. Polli, M. Rini, S. Wall, R. W. Schoenlein, Y. Tomioka, Y. Tokura, G. Cerullo, A. Cavalleri, *Nature Materials* **6**, 643 (2007)
[4] S.L. Johnson, P. Beaud, C. J. Milne, F. S. Krasniqi, E. S. Zijlstra, M. E. Garcia, M. Kaiser, R. Abela, and G. Ingold*et*, *Phys. Rev. Lett.* **102**, 175503 (2009)

**Poster # 16**

# Vibrational control of quantum materials: ultrafast x-ray diffraction studies

A. D. Caviglia[1], M. Först[1], R. Scherwitzl[2], J.-M. Triscone[2], A. Cavalleri[1]

[1]Max Planck Research Department for Structural Dynamics, University of Hamburg - CFEL, Hamburg, Germany
[2]DPMC, University of Geneva, Geneva, Switzerland

## Lattice control

### Static lattice distortions

Functional properties in complex oxides are sensitive to rotation and tilting of oxygen octahedra. It is possible to engineer novel electronic properties by designing and actively controlling such distortions. This can be achieved statically by:

- Chemical and hydrostatic pressure
- Epitaxial strain
- Interfacial structural reconstructions

### Dynamic lattice distortions

Coherent femtosecond mid-infrared pulses can be used to control the lattice structure along a non equilibrium path. Strong vibrational excitation is capable of inducing electronic phase transitions:

- Transformation of the stripe-ordered non-superconducting compound $La_{1.675}Eu_{0.2}Sr_{0.125}CuO_4$, into a transient 3D superconductor [1]
- Insulator-metal transition of charge- and orbital-ordered manganites, $Pr_{0.7}Sr_{0.3}MnO_3$ and $La_{0.5}Sr_{1.5}MnO_4$ [2,3]

## Ionic Raman Scattering

- Excitation of IR active phonons can be used to drive coherently Raman modes such as octahedral rotations. Infrared-active phonon modes can serve as the intermediate state in a Raman scattering process
- Ionic Raman scattering is based on lattice anharmonicities, as opposed to electron-phonon interaction in conventional Raman scattering [5,6]
- This process has recently been observed in $La_{0.7}Sr_{0.3}MnO_3$ [7]

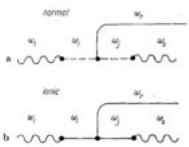

$$H_A = -NAQ_{IR}^2 Q_{RS}$$

### Ionic Raman scattering in the time-domain

- Resonant excitation of the IR-active phonon mode ($Q_{IR}, \Omega_{IR}$) follows

$$\ddot{Q}_{IR} + \Omega_{IR}^2 Q_{IR} = \frac{e^* E_0}{\sqrt{M}_{IR}} \sin(\Omega_{IR} t) F(t)$$

which (for times longer than the pulse width) results in oscillations of the form

$$Q_{IR}(t) = \left[\int_{-\infty}^{+\infty} F(\tau) d\tau\right] \frac{e^* E_0}{\Omega_{IR}\sqrt{M}_{IR}} \cos(\Omega_{IR} t)$$

- With the Hamiltonian HA for IRS the equation of motion for Raman-active phonon modes ($Q_{RS}, \Omega_{RS}$) reads

$$\ddot{Q}_{RS} + \Omega_{RS}^2 Q_{RS} = AQ_{IR}^2$$

i.e., the driving force for the Raman mode is second-order in the coordinate of the resonantly driven IR-active vibration. In the limit of $\Omega_{RS} << \Omega_{IR}$ this induces a ***displacive lattice response analogous to rectification through χ (2) in nonlinear optics***.

$$Q_{RS}(t) = \frac{A}{2\Omega_{RS}^2}\left[\int_{-\infty}^{+\infty} F(\tau) d\tau\right]^2 \frac{\left(e^* E_0\right)^2}{M_{IR}\Omega_{IR}^2}\left(1 - \cos\Omega_{RS} t\right)$$

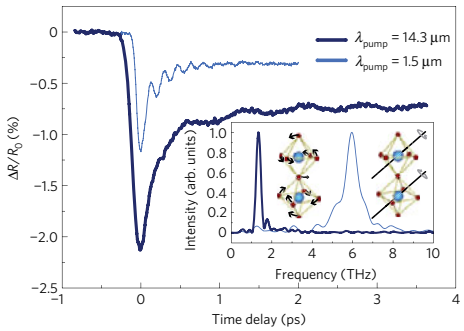


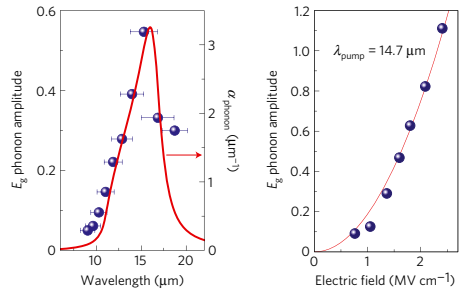


## Proposed experiments

Time-resolved x-ray diffraction can be used to observe the evolution of the lattice as a transient electronic phase is induced by vibrational excitation. It would be particularly interesting to:

- Quantify octahedral rotations as a function of time, using half-order Bragg peaks [4]
- Characterise surface and interfacial structures by monitoring surface truncation rods
- Observe non-linear coupling between phonons

## Experimental requirements

### X-Ray probe beam

- Energy: 6 - 12 keV
- ΔE/E: $10^{-4}$
- Pulse duration < 60 fs
- Photons/pulse > $10^{10}$
- Focus: from 50 to 100 um
- Jitter < 100 fs

### mid-IR pump beam

- Generation by optical parametric amplification (OPA) and difference frequency generation (DFG) of a Ti:sapphire laser amplifier (10 mJ, 800 nm)
- Pulse duration ~ 100 fs
- Energy tunable from 70 to 120 meV (5 meV bandwidth)
- 5 - 10 uJ @ 16 um wavelength
- Focus: from 250 to 300 um

### Experimental station

- Diffraction chamber with cryogenics capabilities down to liquid helium temperatures
- Two-dimensional pixel detector, synchronised to the FEL pulses
- Collinear pump and probe geometry
- Magnetic fields
- Electrical contacts on the sample compatible with high voltages (up to 1kV)

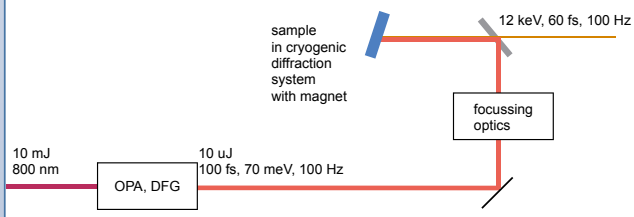


### THz beamline

It would be very beneficial for these experiment to have available a tunable, narrow-band, high intensity (>10 uJ/pulse) THz radiation generated by an undulator. This would be a viable, *jitter-free* alternative to non-linear optics schemes to excite low-energy modes of solids.

## References

[1] D. Fausti et al., *Science* **331**, 189 (2011).
[2] M. Rini et al., *Nature* **449**, 72 (2007).
[3] R.I. Tobey et al., *Phys. Rev. Lett.* **101**, 197404 (2008).
[4] S.J. May, *Phys. Rev. B* **82**, 014110 (2010).
[5] Wallis & Maradudin, *Phys. Rev. B* **3**, 2063 (1971).
[6] Martin & Genzel, *phys. stat. sol. (b)* **61**, 493 (1974).
[7] M. Först et al., *Nat. Phys.* doi: 10.1038/NPHYS2055

## Poster # 17


# Coherent Control of Microscopic Order

## High field THz and X-ray experiments at the SwissFEL

Jeremy A. Johnson, Sebastian Grübel, Simon O. Mariager, Andrin Caviezel, Paul Beaud, Gerhard Ingold

*FEMTO Group, Laboratory for Synchrotron Radiation – Condensed Matter, Paul Scherrer Institut, CH-5232 Villigen, Switzerland*

Teresa Kubacka, Steven L. Johnson

*Institute for Quantum Electronics, ETH Zurich, 8093 Zurich, Switzerland*

THz sources capable of generating MV/cm transient electric field strengths are beginning to allow the investigation of nonlinear responses, and even coherent control, in a host of materials, including processes such as [1]

- carrier cooling
- trapping & recombination
- electron-phonon coupling
- impact ionization
- exciton & polaron dynamics
- Impurity tunneling ionization

There is the exciting possibility of direct coherent control with THz radiation over collective excitations like

- low-frequency phonons
- ferroelectric soft mode
- superconducting gaps in classical BCS superconductors

These and other systems could be insightfully studied with ultrafast X-ray diffraction.

Intense **narrowband** THz has allowed the exploration of anharmonic potential surfaces [2]

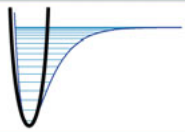

Intense **broadband** THz has been proposed as a means to switch between potential minima [3]

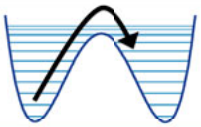

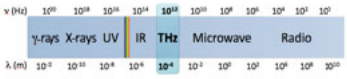


### THz Parameters

| Parameter | | Unit | Requirement/Motivation /Remarks |
|---|---|---|---|
| Broadband THz (half cycle) | frequency | THz | 0.1 - 10 |
| | field strength | MV / cm | 0.1 - 20 |
| Narrowband THz (multicycle) | frequency | THz | 1-20 |
| | pulse width | cycles | 10-20 |
| | | ps (FWHM) | 5 - 20 |
| | jitter | fs (rms) | 5 |
| | | % cycle period | 10 |
| | energy/pulse | μJ | > 10 |

Amplitude phase stable

Whichever is larger

Great flexibility in bandwidth (from broadband to narrowband), polarization, and high field strength of the THz radiation, synchronized with the intense ultrafast X-ray pulses of the proposed SwissFEL, are tantamount to the success of experiments, and could potentially even allow single shot measurements of irreversible processes.

[1] M.C. Hoffmann, J. A. Fülöp. *J. Phys. D: Appl. Phys.* **44**, 083001 (2011).
[2] M. Jeqariya, M. Nagai, K. Tanaka. *Phys. Rev. Lett.* **105**, 203003 (2010).

### X-ray Parameters

| Parameter | | Unit | Requirement | Motivation /Remarks |
|---|---|---|---|---|
| Energy | | keV | 2-12 | High q-space coverage, select edges for resonant diffraction |
| | stability | % | 0.002 | Monochromator required |
| Bandwidth | | % | 0.002 | Monochromator required |
| | stability | % bw | < 10 | |
| Beam position | stability | μm | < 1 | |
| Beam size | | μm | 1 - 200 | Large focus reduces damage at high flux; Grazing incidence requires ~1mm (horiz. only) |
| Photon per pulse | | | $10^{12}$ - $10^{17}$ | Attenuator needed to avoid sample damage |
| | stability | | < | Shot-to-shot normalization with $I_0$ |
| Pulse length | | fs (rms) | 2 | Short pulse mode |
| | stability | % | 10 | |
| Pulse arrival time | stability | fs (rms) | < 5 | With respect to pump laser |
| **Beam parameter changes during experiment** | | | | |
| Energy | range | eV | ±100 | Required for resonant diffraction |
| | step | eV | 0.05 | Required for resonant diffraction |
| | scan | eV / sec | > 1 | Required for resonant diffraction |
| Beam size | | | < | Once per day |
| Pulse length | | | < | Once per day |
| **Beam geometry** | | | | |
| Beam footprint | maximum | mrad | 200 | |
| Working distance | minimum | mm | 500 - 2000 | UHV vacuum chamber, sample rotation, translation, cooling, in-coupling pump laser |

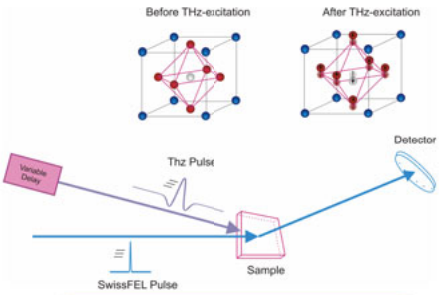


Experimental setup. Accelerator or laser based generation of THz pump pulse excites the system and the resulting ultrafast dynamics are probed via X-ray diffraction

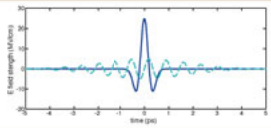

Field strength and spectral brightness of anticipated half cycle or multiple cycle THz pulse

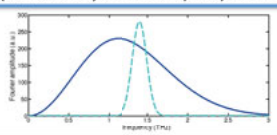

## Study of switching dynamics by broadband THz-radiation induced excitation of prototypic ferroelectric Perovskites

In the context of developing faster and more efficient ways to store information, there has been considerable recent interest on fast switching of the polarization in ferroelectric materials.

Model Case: $PbTiO_3$ [3]

- 2 configurations with opposite polarization
- Switching related to domain reorientation
- Microscopic structure predicted to be drivable with intense electric fields

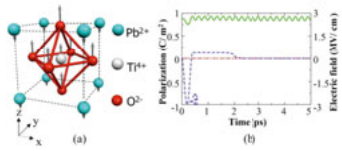


Simulated THz induced switching dynamics of $PbTiO_3$ [3]

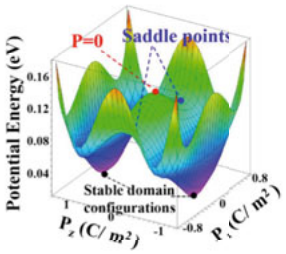


Model Case: $BaTiO_3$ [4]

- Coherent motion of atomic displacements after laser excitation
- Structural changes observed with X-ray diffraction

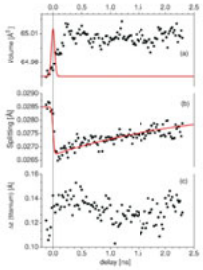


$BaTiO_3$ Unit cell parameters as function of pump-probe delay [4]

Requirements:

- Broadband THz radiation field > 1 MV/cm
- Polarization control
- Detector movable in 3D
- THz/X-ray Single Pulse Measurements

[3] T. Qi, Y. Shin, K. Yeh, K. A. Nelson, A. M. Rappe, *Phys. Rev. Lett.* **102**, 247603 (2009)
[4] K. Isotomin, V. Kotaidis, Q. Kong, A Plech, *Appl. Phys. Lett.* **90**, 022905 (2007)

## Coherent control by narrowband, multiple-cycle THz radiation

Multicycle THz pulses allow efficient energy transfer by tuning to a phonon or magnon resonance frequency of interest. This makes coherent excitation of a selected mode possible.

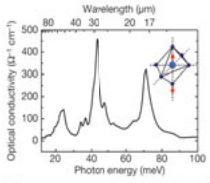


Phonon spectrum in $Pr_{0.7}Ca_{0.3}MnO_3$ [5]

Direct excitation of particular modes with narrowband THz can lead to the whole range of the various phase transitions in different materials.

- **Insulator-to-metal transition** driven by selective excitation of $MnO_6$ tetrahedra stretching mode in $Pr_{0.7}Ca_{0.3}MnO_3$ [5]
- **Superconductivity** induced by IR pumping in $La_{1.675}Eu_{0.2}Sr_{0.125}CuO_4$ [6]

- **Switching between the competing spin-spiral states** predicted to happen under electro-magnon excitation in multiferroic $TbMnO_3$ [7]
- **Magnons** in NiO shown to be controlled even with a short THz pulse [8]

With tunable high-field multi-cycle pulses such dynamics can be investigated in these and other crystals in similar classes of materials.

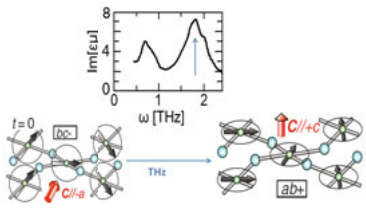


Electromagnon spectrum and switching scheme in $TbMnO_3$ [7]

Requirements:

- Narrowband THz pulse (10 to 20 cycles)
- Control of the sample environment:
  - Temperature: 15 – 700 K
  - Pressure: 0 – 10 GPa
  - Static electric field: 0 – 5 kV
  - Static magnetic field: 0 – 10 T

Future applications:

- Multiferroic memories
- Optospintronics
- Direct manipulation of the crystalline phases

[5] M. Rini et al., *Nature* **449**, 72 (2007)
[6] D. Fausti et al., *Science* **331**, 189 (2011)
[7] M. Mochizuki et al., *Phys. Rev. Lett.* **105**, 147202 (2010)
[8] T. Kampfrath et al., *Nature Photonics* **5**, 31 (2010)